International Journal of Fracture **118:** 303–337, 2002.
© 2003 *Kluwer Academic Publishers. Printed in the Netherlands.*

Choice of standard fracture test for concrete and its statistical evaluation

ZDENĚK P. BAŽANT*, QIANG YU and GOANGSEUP ZI
*Department of Civil Engineering and Materials Science, Northwestern University, Tech-CEE, 2145 Sheridan Rd., Evanston, Illinois 60208, U.S.A (*Author for correspondence: E-mail: z-bazant@northwestern.edu)*

Received 30 October 2001; accepted in revised form 7 January 2003

Abstract. The main characteristics of the cohesive (or fictitious) crack model, which is now generally accepted as the best simple fracture model for concrete, are (aside from tensile strength) the fracture energies G_F and G_f corresponding to the areas under the complete softening stress-separation curve and under the initial tangent of this curve. Although these are two independent fracture characteristics which both should be measured, the basic (level I) standard test is supposed to measure only one. First, it is argued that the level I test should measure G_f, for statistical reasons and because of relevance to prediction of maximum loads of structures. Second, various methods for measuring G_f (or the corresponding fracture toughness), including the size effect method, the Jenq-Shah method (TPFM), and the Guinea et al. method, are discussed. The last is clearly the most robust and optimal because: (1) it is based on the exact solution of the bilinear cohesive crack model and (2) necessitates nothing more than measurement of the maximum loads of notched specimens of one size, supplemented by tensile strength measurements. Since the identification of material fracture parameters from test data involves two random variables, f'_t (tensile strength) and G_f, statistical regression should be applied. But regression is not feasible in the original Guinea et al.'s method. The present study proposes an improved version of Guinea et al.'s method which reduces the statistical problem to linear regression thanks to exploiting the systematic trend of size effect. This is made possible by noting that, according to the cohesive (or fictitious) crack model, the zero-size limit σ_{N0} of nominal strength σ_N of a notched specimen is independent of F_f and thus can be easily calculated from the measured f'_t. Then, the values of σ_{N0} obtained from the measured f'_t values, together with the measured σ_N-values of notched specimens, are used in statistical regression based on the exact size effect curve calculated in advance from the cohesive crack model for the chosen specimen geometry. This has several advantages: (1) the linear regression is the most robust statistical approach; (2) the difficult question of statistical correlation between measured f'_t and the nominal strength of notched specimens is bypassed, by virtue of knowing the size effect trend; (3) the resulting coefficient of variation of mean G_f is very different and much more realistic than in the original version; (4) the coefficient of variation of the deviations of individual data from the regression line is very different from the coefficient of variation of individual notched test data and represents a much more realistic measure of scatter; and (5) possible accuracy improvements through the testing of notched specimens with different notch lengths and the same size, or notched specimens of different sizes, are in the regression setting straightforward. For engineering purposes where high accuracy is not needed, the simplest approach is the previously proposed zero-brittleness method, which can be regarded as a simplification of Guinea et al.' method. Finally, the errors of TPFM due to random variability of unloading-reloading properties from one concrete to another are quantitatively estimated.

Key words: Cohesive crack model, standard fracture test, concrete.

1. Introduction

Since the mid 1980s, the question of a proper fracture test standard for concrete and other quasibrittle materials has been intensely debated (e.g., Bažant and Planas, 1998). Three vital aspects, however, have not received proper attention: (1) the differences in the statistical scatter of measurements of various fracture characteristics, (2) the method of statistical evaluation, and (3) the relevance to the prediction of load capacities of fracturing structures. The last

aspect is, in most cases, a more important objective in design than the prediction of post-peak softening behavior of structures. All these three aspects will be addressed in the present study. The best available testing method will be identified and its improved, more effective version, will be formulated.

The basic premise of the present analysis is that the best available fracture model for concrete is the cohesive crack model (or the crack band model, which is based on it and is essentially equivalent). The cohesive crack model was developed in the works of Barenblatt (1959, 1962), Leonov and Panasyuk (1959), Rice (1969), Palmer and Rice (1973), Knauss (1973, 1974), Smith (1974), Wnuk (1974) and Kfouri and Rice (1976). For concrete, it was pioneered and generalized by Hillerborg et al. (1976) under the name fictitious crack model.

As usual in studies with the cohesive crack model, we consider the softening curve of cohesive (crack-bridging) stress versus the separation (opening displacement) to be monotonically decreasing and smooth, and to have an initial tangent of a finite negative slope (Hillerborg et al., 1976; Petersson, 1981; Hillerborg, 1983, 1985a,b; Bažant and Planas, 1998). There exist models in which the initial tangent is assumed to be rising. But such an assumption inevitably leads to self-contraction since the tensile stresses in the bulk material at points sufficiently close to the crack face and to the tip inevitably exceed the tensile strength if this assumption is made. Some authors assume a softening curve with a long horizontal initial segment, but such an assumption is appropriate only for ductile metals, and not quasibrittle materials. Nevertheless, the available measurements do not suffice to exclude the possibility of a horizontal initial tangent or even a short initial horizontal segment on the softening curve, nor the possibility of a piece-wise constant softening curve, consisting of a series of downward steps. In practice, though, these questions are moot because the inevitable scatter of test data does not allow determining the very initial slope and the detailed subsequent shape of the softening curve precisely. Of course one could assume various softening curves with or without a very short initial horizontal segment, as well as step-wise or oscillating curves, but in order to fit all the existing test data they would have to globally resemble the well-known bilinear curve (Guinea et al., 1994a,b). For these reasons, it is not unduly restrictive to assume the entire softening curve to be bilinear (Figure 1). The initial slope of this bilinear curve should of course be understood as merely the average slope of the actual cohesive response during the reduction of cohesive stress to about 1/3 of the tensile strength.

This study will first attempt to identify the desired objectives of fracture testing of concrete and then discuss and compare various testing methods. Taking into account the fact that the response of a specimen of vanishing size depends only on the tensile strength (and not on the softening stress-separation curve of the cohesive crack model) will lead to an improvement of the best existing method, Guinea et al.'s method, by which the identification of G_f and other fracture parameters can be reduced to statistical linear regression. The arguments will be supported by extensive statistical simulations.

2. Difference in physical meanings of fracture energies G_f and G_F

Usually there are not enough test data for a given concrete to determine all the four parameters of the bilinear softening curve. So the shape of the softening curve is assumed as fixed, i.e., the ratio of slopes of the first and second straight segments and the relative height of the point of slope change in Figure 1 are assumed a priori, and then the softening curve is characterized by only two parameters. One is normally taken as the tensile strength f'_t, and the other can be chosen in various equivalent ways, for example as either:

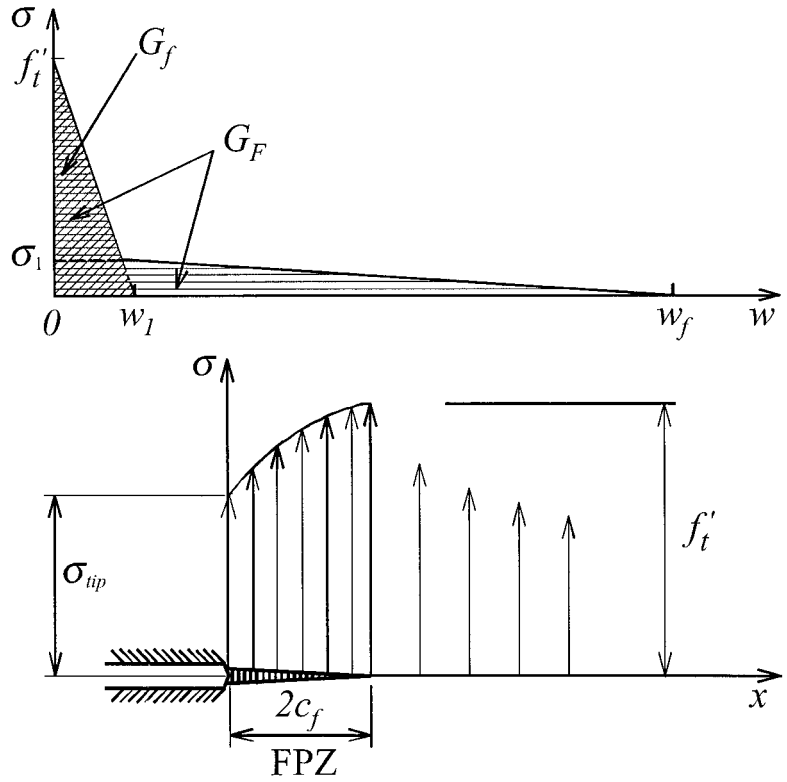

Figure 1. Top: Bilinear softening stress-separation curve of cohesive crack model. Bottom: Typical stress profile (at maximum load) throughout the fracture process zone in a notched test specimen of positive geometry.

1. the *total* fracture energy G_F, representing the area under the complete curve (Rice, 1969; Hillerborg et al., 1976; Petersson, 1991; Hillerborg, 1983, 1985a,b), or
2. the *initial* fracture energy G_f, representing the area under the initial tangent of the softening curve (Elices and Planas, 1992; Guinea et al., 1992) (Figure 1).

The fracture energies G_f and G_F are of course two different material characteristics, which are only weakly correlated. G_F can be estimated from G_f and *vice versa*, but not at all accurately. Ideally, both G_f and G_F should be measured and used for calibrating the initial slope and the tail of the softening curve of the cohesive crack model (or the crack band model, which is nearly equivalent; Bažant and Oh, 1983). For concrete, as a very rough approximation,

$$G_F/G_f \approx 2.5 \tag{1}$$

as reported by Planas and Elices (1992) and further verified statistically by Bažant and Becq-Giraudon (2001, 2002a). Knowing this ratio, one can calibrate a bilinear softening curve, provided that the relative height σ_1 of the 'knee' (the point of slope change, Figure 1 top) is also known.

The ratio $G_F/G_f = 2.5$, however, is doubtless a rather crude estimate. Properly, it should be regarded as a random quantity. The coefficient of variation of the ratio G_F/G_f may be roughly guessed as perhaps

$$\omega_{Ff} \approx 40\% \tag{2}$$

For infinite-size specimens, the cohesive stress at notch tip under maximum load vanishes and thus the maximum load is decided by G_F rather than G_f (e.g., Bažant and Pfeiffer,

1987; Bažant and Kazemi, 1991). However, for normal-size fracture specimens (as well as most concrete structures in practice), the maximum load of notched fracture specimens is determined by G_f. The reason is that these specimens are not large enough, by far, for the cohesive stress at maximum load to be reduced to zero. In fact, as shown first by Guinea et al. (1994a,b) and verified later in this study the cohesive stress is reduced at maximum load to only about 50% to 75% of f_t' (this is even true of most concrete structures built). Therefore, the maximum loads of notched specimens (as well as most structures) depend only on the initial tangent of the softening stress-separation curve, which is fully characterized by G_f (Bažant and Planas, 1998). They are independent of the tail of the softening curve.

On the other hand, the prediction of the entire postpeak softening load-deflection curve of a specimen or structure depends strongly also on the tail of the stress-separation curve of the cohesive crack model, and thus on G_F.

3. Statistical scatter of G_f and G_F, and mean trends

An important consideration for the choice of fracture test is the statistical scatter of the measured quantity. As it is well known, the mean of a stochastic variable can usually be estimated with only about 6 tests. However, for a meaningful determination of the standard deviation, the number of tests must be of the order of 100. There is no test data set of that scale in the literature, for neither G_f nor G_F. Besides, even if such a data set were available, its usefulness would be limited because it would be difficult to infer from it the standard deviations for concretes of a different composition, curing, age and hygrothermal history.

Thus, if we wish to gain any statistical information, it is inevitable to study the fracture test data for all concretes. Here the situation has become rosy: While a dozen years ago only about a dozen test series were available in the literature, Bažant and Becq-Giraudon (2001, 2002) collected from the literature 238 test series from different laboratories throughout the world, conducted on different concretes. Of these, 77 test series concerned G_f (or the related fracture toughness K_c), and 161 G_F. However, to be able to extract any statistics from these data, the basic deterministic trends must somehow be filtered out first, at least approximately.

One must, therefore, first establish the formulae that approximately describe the deterministic (mean) dependence of G_f and G_F on the basic characteristics of concrete. Using extensive nonlinear optimization studies based on the Levenberg–Marquardt algorithm, Bažant and Becq-Giraudon (2001, 2002) obtained two simple approximate formulae[1] for the means of

[1] These formulae read:

$$G_f = \alpha_0 (f_c'/0.051)^{0.46} \left[1 + (d_a/11.27)\right]^{0.22} (w/c)^{-0.30}; \qquad \omega_{G_f} = 17.8\% \tag{3}$$

$$G_F = 2.5\,\alpha_0 (f_c'/0.051)^{0.46} \left[1 + (d_a/11.27)\right]^{0.22} (w/c)^{-0.30}; \qquad \omega_{G_F} = 29.9\% \tag{4}$$

$$c_f = \exp\left\{\gamma_0 (f_c'/0.022)^{-0.019} \left[1 + (d_a/15.05)\right]^{0.72} (w/c)^{0.2}\right\}; \qquad \omega_{c_f} = 47.6\% \tag{5}$$

Here $\alpha_0 = \gamma_0 = 1$ for rounded (river) aggregates, while $\alpha_0 = 1.44$ and $\gamma_0 = 1.12$ for crushed or angular aggregates; ω_{G_f} and ω_{G_F} are the coefficients of variation of the ratios G_f^{test}/G_f and G_F^{test}/G_F, for which a *normal* distribution may be assumed, and ω_{c_f} is the coefficient of variation of c_f^{test}/c_f, for which a *lognormal* distribution should be assumed (ω_{c_f} is approximately equal to the standard deviation of $\ln c_f$). The fracture toughness and the mean critical crack-tip opening displacement, used in the Jenq-Shah method (TPFM), are then estimated as

$$K_c = \sqrt{E' G_f}, \qquad \delta_{\text{CTOD}} = \sqrt{32 G_f c_f / \pi E'} \tag{6}$$

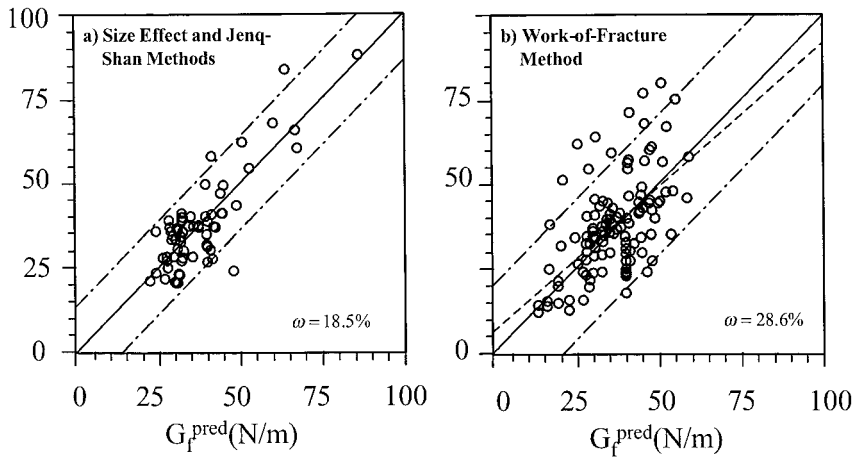

Figure 2. Plots of measured versus predicted values of fracture energy G_f or G_F, obtained by (a) peak-region methods (SEM, TPFM, ECM, 77 data). (b) Work-of-fracture method (161 data) (note: ω = coefficient of variation of vertical deviations of data points from regression line).

G_f and G_F (as well as c_f, the effective length of the fracture process zone) as functions of the compressive strength f'_c, maximum aggregate size d_a, water-cement ratio w/c and aggregate shape. The optimization studies confirmed that the aforementioned ratio $G_F/G_f = 2.5$ is statistically nearly optimum and that it displays no systematic dependence on f'_c, d_a and w/c.

Based on these mean predictions formulae, plots of the measured versus predicted values of G_f and G_F (as well as c_f) were constructed (see Figure 2). The coefficients of variation of the vertical deviations of the data points from the straight line of slope 1 (i.e., the line representing the case of perfect prediction by the deterministic formula) were found to be

$$\omega_{G_f} = 18.5\% \quad \text{for} \quad G_f, \qquad \omega_{G_F} = 28.6\% \quad \text{for} \quad G_F. \tag{7}$$

The large difference between these two values has significant implications for the choice of the testing standard, which we will discuss later.

It must, of course, be admitted that the errors of the prediction formulae for G_f and G_F, which are owed mainly to limitations in our current understanding of the effects of concrete composition, make doubtless major contributions to the aforementioned high values of the coefficients of variations. However, there is no reason why these contributions should be biased in favor of G_f or G_F. Eliminating the mean trend by an imperfect prediction formula is inevitable if any statistical comparisons at all should be made at the present level of experimental evidence. Therefore, we must accept that the difference between these two coefficients of variation characterizes, at least in a crude approximate manner, the difference in the inherent random scatter of either G_f and G_F, or their measurement methods, or (more likely) both.

Why do the data on G_F (Figure 2 right) exhibit a much higher scatter than those on G_f? The reasons appear to be: (1) An inherently higher randomness of the tail compared to the initial portion of the softening curve; (2) uncertainty in extrapolating the tail to zero stress; and (3) the difficulties in eliminating from experimental measurements various non-fracture sources of energy dissipation and the effects of specimen size and shape (Planas et al., 1992).

The fracture parameters measured by the size effect method have the advantage that they are, by definition, size and shape independent, provided of course that the correct size effect law with shape dependent coefficients is known, for the given size range.

4. Basic testing methods

Among the available experimental methods of measuring the fracture properties of concrete (Bažant and Planas, 1998, Section 7.2.2 and Section 7.3), three basic classes may be distinguished:

1. The *peak-load methods*, which rely on measuring only the maximum loads and exist in two variants:
   (a) The *size effect method* (SEM) (Bažant, 1987; Bažant and Pfeiffer, 1987; RILEM, 1990; Bažant and Kazemi, 1991), which is implied by the size effect law (Bažant, 1983, 1984) and requires testing notched specimens of at least two sufficiently different sizes (preferably with dissimilar notches, Bažant, 2002a).
   (b) The *notched-unnotched method* (NUM), developed by Guinea et al. (1994a,b), which necessitates testing (i) a notched fracture specimen (of one size) and (ii) an unnotched specimen, the latter recommended to be the splitting cylinder for the Brazilian test.
2. The *peak-region methods*, in which all the measurements are taken in the maximum load region but more than just the maximum load needs to be measured. This class includes mainly the *Jenq–Shah method*, which is also called the *two-parameter fracture model* (TPFM) (Jenq and Shah, 1985; RILEM, 1990) and represents an adaptation to concrete of Wells' (1965) and Cottrell's (1963) method for metals. This method requires also measurements of the unloading compliance and of the crack-tip opening displacement δ_{CTOD}. [Further in this class one could mention the effective crack model (ECM) developed by Nallathambi and Karihaloo (1986), and Karihaloo and Nallathambi (1989a,b, 1991), which however is not a general model, being formulated only for notched beams.]
3. The *complete-curve methods*, in which the complete load-deflection curve of the specimen is directly measured. This includes mainly:
   (a) the work-of-fracture method, also known as Hillerborg's method (Hillerborg et al., 1976; Hillerborg, 1983, 1985; RILEM, 1985), which was originally developed for ceramics (Nakayama, 1965; Tattersall and Tappin, 1966) and is based on measuring the work done on fracturing the whole ligament of a notched specimen; and also
   (b) the *direct tensile test method*, in which one tries to maintain, over the whole cross section and during the entire test, a uniform crack opening so that the cohesive stress could be inferred from the measured load.

In the mid-1980s, there existed what appeared to be three good test methods for fracture of concrete – Hillerborg's method, the Jenq–Shah method, and the size effect method. Their relative merits still not completely clear, they were all embodied in RILEM international standard recommendations (RILEM, 1985, 1990a,b). In the early-1990s it was realized that the last two yield a different fracture energy (G_f) than the first (G_F). Further it was realized that the Jenq–Shah method suffers from a certain theoretical inconsistency while being less simple than Guinea et al.'s method (as explained later) and providing no additional information. As for the size effect method, its experimental simplicity and the possibility of statistical parameter identification through linear regression crystallized as its strongest points, however, the need of fabricating test specimens of different sizes has been seen as a disadvantage by many experimenters, while its accuracy in determining G_f is not very high unless inconveniently

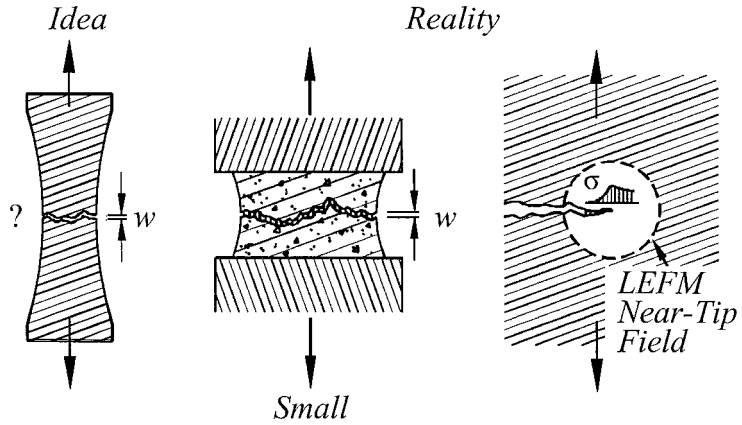

Figure 3. Left: The idea of direct measurement of the softening stress-separation curve. Middle: specimen needed to achieve nearly simultaneous separation. Right: field surrounding the FPZ in a large structure.

large specimens are used. The work-of-fracture method is well understood and discussed in depth elsewhere (e.g., Bažant and Planas, 1998). The direct tensile test method is plagued by serious difficulties.[2] Therefore, our analysis of testing methods will from now on focus on NUM (Guinea et al.'s method) and its improvement through exploiting the simple statistical linear regression approach of the size effect method.

The optimal choice of test specimens for Guinea et al.'s method is an important question. For the test of tensile strength f'_t, Planas and Elices (Bažant and Planas, 1998, Section 7.3.1) recommend (on the basis of the tests of Rocco, 1996) the Brazilian split-cylinder test. For that test, as they observe, the pre-peak nonlinearity has a lesser spoiling influence than it has for other tensile strength tests. The type of notched specimens is best chosen so as to maximize the brittleness number, as discussed in Bažant and Li (1996). Although these question may deserve further discussion, they are beyond the scope of the present analysis, which is independent of the choice of specimen type.

5. Level I and level II testing

At the (pre-FraMCoS-2) workshop of American and European specialists in Cardiff in 1995 (organized by B.I.G. Barr and S.E. Swartz) it was agreed that the testing standard should specify two levels of testing:

[2]If the direct tensile specimen is large enough to allow the FPZ to develop over its length and width without interference of the boundaries (Figure 3 left), the crack separation does not proceed simultaneously over the cross section; the specimen inevitably flexes sideway at least slightly and the fracture propagates across the cross section. To avoid it, it has been attempted to use very short specimens bonded to very stiff platens close to the crack, loaded through a very stiff frame (Figure 3 center). Then a (statistically) uniform separation can be achieved but the $\sigma(w)$ curve that is measured is not relevant for real structures because the FPZ development is hindered by the boundaries and affected by their geometry. The unique $\sigma(w)$ curve that characterizes a FPZ developed fully, without hindrance, can be obtained only if the field of stress and strain around the FPZ is independent of geometry and size (Figure 3 right). Unfortunately, this can be achieved only if the specimen is large, much larger than the FPZ, in which case the FPZ in a large enough specimen is surrounded by the LEFM near-tip asymptotic field, which is always the same, regardless of geometry. This field does not surround the FPZ in a short direct tension specimen with platens close to the crack.

- At level I, acceptable for structures of not too high fracture sensitivity, it should suffice to measure only one of the two fracture energies, either G_F or G_f.
- At level II, appropriate for structures of high sensitivity to fracture and size effect, both G_F and G_f (or K_c) should be directly measured.

If the cohesive crack model is calibrated by a level I test, one must of course assume in advance the shape of the softening-stress separation curve, i.e., fix the ratios G_F/G_f and σ_1/f_t' based on prior knowledge (Figure 1). Therefore,

- if G_f is measured, and if the tail of the softening curve is needed, one must use the estimate $G_F \approx 2.5G_f$; and
- if G_F is measured, one must use the estimate $G_f \approx 0.4G_F$, and from that determine the initial slope of the softening curve.

6. Level I test: measure G_f or G_F?

There is a widespread tendency to measure only one of the two fracture energies. In that case, if the cohesive crack model is to be used in structural analysis, the shape of the stress-separation diagram must be fixed in advance. If a bilinear softening diagram is adopted, this for example means fixing the ratios G_F/G_f and σ_1/f_t' (Figure 1).

Most civil engineers have so far preferred using only G_F. This might be explained by the fact that the work-of-fracture method and the use of the cohesive crack model in finite element programs can be understood even by civil engineers who have received no education in fracture mechanics. The same cannot be said about the NUM, SEM or TPFM. Although these methods, too, can be used by an engineer with no such education, their understanding does require at least an elementary acquaintance with fracture mechanics. However, the choice of the testing standard should not harmed by the inadequacy of the current civil engineering curricula (rather, the curricula should be modernized).

The prime criterion should be that of accuracy, of minimizing the statistical uncertainty in structural analysis and design. According to (7), the answer is clear – *level I should involve the testing of G_f, and G_F should then be estimated from G_f,* e.g., *as $G_F \approx 2.5G_f$*. The reason can further be documented as follows.

Because level I testing necessitates the ratio G_f/G_F to be fixed, the coefficient of variation of errors of the fracture energy that is measured will get imposed on the other fracture energy that is inferred. Considering G_F and the ratio G_f/G_F as two independent random variables, the coefficient of variation of G_f predicted from G_F will be

$$\omega_{G_f} \approx \sqrt{0.286^2 + 0.40^2} = 49\% \tag{8}$$

The maximum load of a structure, $P_{\max}$, is approximately proportional to K_c, and since $K_c \propto \sqrt{G_f}$, it is approximately proportional to $\sqrt{G_f}$.

Therefore, if the level I test measures only G_F, the coefficient of variation of the predicted maximum load of a structure (even if calculated accurately with the cohesive crack model) will be about

$$\omega_{P_{\max}} \approx 49\%/2 \approx 25\% \tag{9}$$

because $P_{\max} \propto \sqrt{G_f}$.

On the other hand, if the level I test measures directly G_f, then

$$\omega_{P_{\max}} \approx 18.5\%/2 \approx 9\% \tag{10}$$

Compared to 25%, this is a huge superiority in accuracy, which cannot be ignored in the choice of level I test.

The values of the coefficients of variation considered above apply for normal practice in which only a few tests (say, 6) of the given concrete are carried out in the level I test. In that case only the mean measured value is statistically realistic but measurements of ω_{G_F} or ω_{G_f} are not.

In the special case that many, say 100, fracture tests of the given concrete by the chosen level I method are performed, the values of the coefficients of variation of fracture energy, ω_{G_F} and ω_{G_f}, can be meaningfully calculated from the tests of the given concrete alone. Those values may be expected to be considerably smaller than the preceding values because concretes of different compositions are not mixed within one set. But both coefficients of variation will likely be reduced by the same ratio, say, to $\omega_{G_F} = 20\%$ and $\omega_{G_f} = 12\%$. Consequently, the advantage of using G_f rather than G_F for the level I test will be preserved.

Based on the foregoing analysis, the direct measurement of G_f (or K_c), rather than G_F, is obviously a much better choice for the level I test. But an additional point to consider is that of simplicity.

The measurement procedure for obtaining only the peak loads is clearly simpler than the measurement procedure of the Jenq–Shah method. It is foolproof, and feasible even with the most rudimentary testing equipment. A stiff testing frame and closed-loop servo-control are not needed, in principle, however they are nevertheless desirable in order to avoid unnecessary errors due material rate sensitivity (because a rapid creep on approach to the peak load can greatly change the loading rate). Another point to note is that the crack band model, the only fracture model used by the civil engineering firms and commercial codes, requires as input the values of G_f and f_t'. If K_c and δ_{CTOD} are given, they must be converted to G_f, which involves an additional error.

For these reasons, our discussion will henceforth focus on the peak-load methods.

7. Review of relationship between size effect law and fracture parameters

The classical size effect law and the expressions for its coefficients read as follows:

$$\sigma_N = \sigma_0 \left(1 + \frac{D}{D_0}\right)^{-1/2} = \sqrt{\frac{E' G_f}{g'(\alpha_0) c_f + g(\alpha_0) D}}, \tag{11}$$

where

$$\sigma_0 = B f_t', \qquad D_0 = \ell_1 / B^2 g(\alpha_0) \tag{12}$$

(Bažant, 1984, 1987; Bažant and Pfeiffer, 1987; Bažant and Kazemi, 1991). Here $\sigma_N = P_{\max}/bD$ = nominal strength of structure (parameter of applied load having the dimension of stress), $P_{\max}$ = maximum load, b = specimen width, D = characteristic specimen size (usually taken as the cross section dimension); $E' = E/(1 - \hat{\nu}^2)$ = elastic modulus for plane strain (E = Young's modulus, $\hat{\nu}$ = Poisson ratio); σ_0 = nominal strength extrapolated to zero size ($D \to 0$) according to the classical size effect law, f_t' = direct tensile strength of material, B = geometry constant, depending on specimen geometry; D_0 = transitional size; c_f = effective length of fracture process zone (about a half of the actual process zone length

at maximum load for a very large specimen); $g(\alpha) = k^2(\alpha)$ = dimensionless LEFM energy release function, $\alpha = a/D$ = relative crack length (up to the front of the fracture process zone, i.e., the cohesive zone), $\alpha_0 = a_0/D$, a_0 = length of the notch (or a fatigued crack); and $k(\alpha) = K_I/\sigma_N\sqrt{D}$ = dimensionless stress-intensity factor ($K_I = \sqrt{E'G_f}$ = stress intensity factor); furthermore

$$\ell_1 = E'G_f/f_t'^2 = B^2 g'(\alpha_0)c_f \tag{13}$$

represents the characteristic length of the material corresponding to G_f (to be distinguished from characteristic length $l_0 = E'G_F/f_t'^2$ corresponding to G_F).

In the size effect method, the maximum load data (for specimens with a sufficiently broad range of brittleness numbers $\beta = D/D_0$) are fitted with the size effect law. Although direct data fitting in the plot of $\log\sigma_N$ versus $\log D$ has some statistical advantages (Bažant and Planas, 1998), the simplest way is to use linear regression, exploiting the fact that, in a plot of $Y = 1/\sigma_N^2$ versus $X = D$, the size effect law (11) appears as a straight line, $Y = AX + C$. Once the slope A and the intercept C have been evaluated, constants D_0 and $\sigma_0 = Bf_t'$ can be determined as

$$\sigma_0 = 1/\sqrt{C}, \qquad D_0 = C/A = \ell_1/B^2 g(\alpha_0). \tag{14}$$

Then the fracture energy, the effective process zone length and the tensile strength of cohesive crack model can be obtained as

$$G_f = \frac{\sigma_0^2}{E'} D_0 g(\alpha_0), \qquad c_f = D_0 \frac{g(\alpha_0)}{g'(\alpha_0)}, \qquad f_t' = \frac{\sigma_0}{B}. \tag{15}$$

8. Notched-unnotched method of Guinea, Planas and Elices (NUM)

Although one of the derivations of the size effect law rests on a large-size asymptotic expansion of the cohesive crack model, the maximum load values calculated with the cohesive crack model deviate from this law appreciably if the test specimens are too small. But in testing, we of course want to use as small specimens as possible. To permit the use of the smallest possible specimens, it is therefore preferable to fit the maximum load data directly with the cohesive crack model. Besides, for the sake of ease of testing, it is desirable to avoid the need for testing notched specimens of different sizes. An ingenious way to satisfy both aims has been devised by Guinea et al. (1994a,b), as follows.

With a justification to be given later, it is assumed that the maximum load of a notched specimen is governed only by the initial tangent of the softening curve of the cohesive crack model. This means that a linear softening can be assumed for calculations, which is a great simplification. Under that assumption, the exact curve of σ_N/f_t' versus D/ℓ_1 is numerically computed in advance for the recommended test geometry. By fitting the computational results, an explicit analytical expression (sufficiently accurate within the range of testing, assumed to be limited to $0.25 \leq \sigma_N/f_t' \leq 0.54$) is obtained in advance by using the inverse relation (Bažant and Planas, 1998, Equation 7.3.2):

$$D/\ell_1 = \chi(\sigma_N/f_t') \tag{16}$$

where function χ for the given specimen geometry is defined by a polynomial approximation of accurate cohesive crack computations for the given specimen geometry (Bažant and Planas,

1998, Equations 7.3.4–7.3.5). The method of Guinea et al. (1994a,b) may be summarized as follows:

Method A.

1. From the mean $\bar{\sigma}_N$ of the measured values of the nominal strength σ_N of notched concrete specimens, and the mean $\bar{f}'_t$ of the measured tensile strength f'_t of concrete, calculate:

$$\ell_1 = D / \chi(\bar{\sigma} / \bar{f}'_t) \tag{17}$$

2. Then, using the mean measured value $\bar{E}'$ of modulus E', estimate the mean fracture energy

$$\bar{G}_f = \ell_1 (\bar{f}'_t)^2 / \bar{E}' \tag{18}$$

The coefficient of variation of G_f as a smooth function of three random variables σ_N, f'_t and E' (considered as independent) may then be roughly estimated as

$$\omega_{G_f} = \sqrt{{\omega_{\sigma_N}}^2 + {\omega_{f_t}}^2 + {\omega_E}^2} \tag{19}$$

where ω_{σ_N}, ω_{f_t} and ω_E are the coefficients of variation of σ_N, f'_t and E'. Thus, only the tests of tensile strength and the tests of the maximum load of notched specimens of one size and one geometry are needed to determine G_f and estimate its coefficient of variation. Nothing can be simpler than that.

9. Should size effect be exploited?

In method A as well as Guinea et al.'s method, a question arises as to the optimal statistical evaluation as well as possible accuracy improvement based on testing notched specimens of different sizes or geometry. The original version allows considering the statistical scatter only with respect to the notched nominal strength σ_N. But there are two random input variables in the problem, σ_N and f'_t, and their statistical correlation is a difficult question with uncertain answer. There are also two stochastic material parameters to identify, G_f and f'_t. In that case, statistical regression should always be preferred, provided of course that σ_N and f'_t can be related through some systematic trend.

Such a systematic trend indeed exists – it is furnished by the size effect properties of the cohesive crack model. It has been mathematically demonstrated (Bažant 2001) that if the structure size tends to zero, the asymptotic load capacity of any structure (notched or notchless) failing through a cohesive crack depends only on the tensile strength f'_t of the material, and not on G_f nor any other characteristic of the softening stress-separation curve. Therefore, as long as the cohesive crack model is accepted as a valid model, the tensile strength data are equivalent to the maximum load data of the notched specimen extrapolated to zero size (Bažant and Li 1996).

The classical size effect law (Bažant 1984) is reducible to linear regression – the most robust statistical approach. Consequently, linear regression can be achieved by modifying the experimental σ_N values according to the deviations of the exact cohesive size effect curve from this classical law. The main advantage is that the existence of the underlying size effect trend, permitting linear regression, eliminates the difficult question of statistical correlation

between f_t' and G_f. This correlation is significant and would have to be tackled if the size effect trend were unknown, despite the fact that the cvalue of the correlation coefficient is notoriously uncertain.

10. Exact size effect curve of cohesive crack model

We consider only test specimens of positive geometry (Bažant and Planas, 1998), in which the cohesive zone (i.e., the fracture process zone) is at the maximum load still attached to the notch tip. Asymptotically, for a specimen of infinite size, the fracture process zone is, at maximum load, fully developed, i.e., the cohesive stress value at the notch tip, σ_{tip}, vanishes. But this is far from true for normal finite-size concrete specimens.

It is obvious that the second linear segment of the softening curve (Figure 1) is reached only if the crack opening w at the notch tip under the maximum load is sufficiently large. Guinea et al. (1994a,b) showed that this situation is not reached for most normal-size concrete fracture test specimens and, consequently, all the stress states along the entire cohesive crack lie, at maximum load, still on the first linear segment of the softening curve (Figure 1). This observation, which is here verified computationally, makes it possible to identify G_f from the maximum load data alone (Guinea et al. 1994a,b).

The size effect curves corresponding to the bilinear cohesive crack model have been computed (with three-digit accuracy) for various test geometries using the eigenvalue approach. In this approach, the size D for which a given relative length of the cohesive crack gives the maximum load is obtained as the eigenvalue of a certain homogeneous Fredholm integral equation (Bažant and Li, 1996; Bažant, 2002b; see Equation (7.5.37) in Bažant and Planas, 1998), which has been solved numerically with high accuracy.

Computations have been run for four basic types of fracture specimens shown in Figures 4 and 5, which include ligaments loaded in pure tension, tension with bending and pure bending. The results are presented in these figures as the dimensionless plots of η versus ξ where

$$\eta = (f_t'/\sigma_N)^2, \qquad \xi = D/\ell_1 \tag{20}$$

(the characteristic size D is defined for the present calculations as the dimension of the cross section; see the specimen sketches in Figures 4 and 5). The small-size behavior is emphasized in Figure 6 which presents the initial portions of the same plots in an expanded size coordinate. Figures 9a and 9b illustrate the difference between the size effect law matched to the test data and the asymptote of the cohesive crack model. Figures 7 and 8 show the same results plotted in coordinates that make conspicuous the asymptotic small-size and large-size behaviors. For large sizes D, the plots in Figures 4 and 5 approach a straight-line asymptote (shown dashed in the figures), which represents the large-size asymptotic behavior of a linear cohesive crack model in which the initial linear softening stress-separation diagram, extended down to zero stress, delimits area G_f.

Note that Guinea et al.'s (1994a,b) hypothesis is indeed verified: Throughout the entire size range of all the plots, the cohesive stress σ_{tip} at the notch tip is higher than the stress σ_1 (Figure 1) corresponding to the slope change of the bilinear softening stress-separation diagram (it is in fact higher than σ_1 for a size range much broader than the range of interest shown in the plots). Therefore, the straight-line asymptote of a smooth extension of these plots must correspond to G_f rather than G_F.

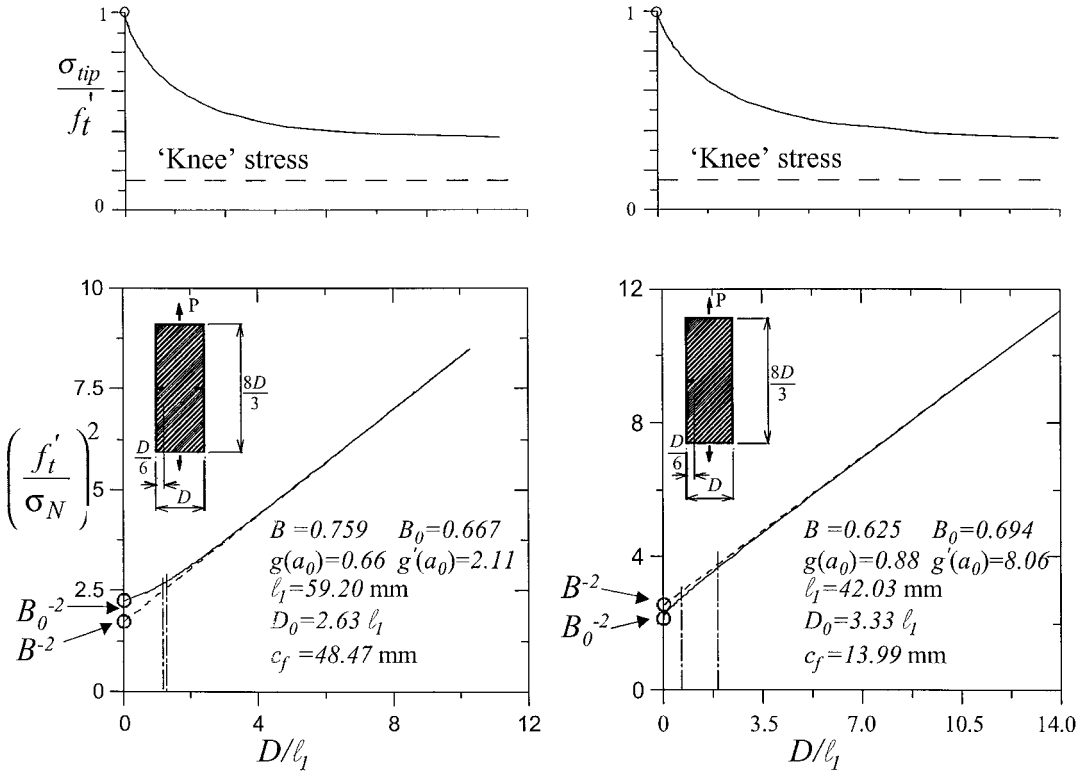

Figure 4. Bottom: Dependence of σ_N^{-2} of singly and doubly notched tensile specimens on size D, calculated from bilinear cohesive crack model for various specimen geometries (the straight dashed line in these plots is the size effect asymptote). Top: dependence of notch-tip stress σ_{tip} on D.

So we have confirmed that the maximum loads of normal laboratory specimens (as well as normal structures) indeed depend only on G_f. In other words, G_F is irrelevant for maximum loads.

The values of the ratios $B = \sigma_0/f_t'$ and $B_0 = \sigma_{N0}/f_t'$ will be useful for our analysis and are indicated in the figures; σ_0 denotes the zero-size stress value for the straight asymptote and σ_{N0} denotes the zero-size stress value computed from the initial linear segment of the softening cohesive curve (Figure 10) (the value σ_{N0} can be easily obtained by hand-held calculator as the nominal strength of a specimen with a plastic 'glue' in the crack plane; see Appendix I).

The computed graphs in Figures 4–6 are curved but, compared to the inevitable experimental errors, their deviation from the dashed asymptote is rather small for a rather broad size range. The limit of this range, marked in the figures as D_e, may be defined as the size D for which $\Delta\sigma_N$ is 3% of σ_N, which is negligible compared to the typical experimental scatter.

Since the structural analysis methods are based on continuum concepts such as the stress and strain, the cross section must be large enough compared to the maximum aggregate size d_a in order for these concepts to make sense. In this regard, the minimum cross section dimension of test specimen, $D = D_{\min}$, should be about $6d_a$ (however, $D = 12d_a$ gives better accuracy, while $3d_a$ can be used for crude analysis). Although the plots are dimensionless and valid for any G_f and f_t', the calculation results have been matched to the test data reported by Bažant and Pfeiffer (1987) and He et al. (1992) in order to ascertain the value of the dimensionless parameter $D_{\min}/\ell_1$ of $6d_a/\ell_1$ for each practical test geometry. This value is marked in each

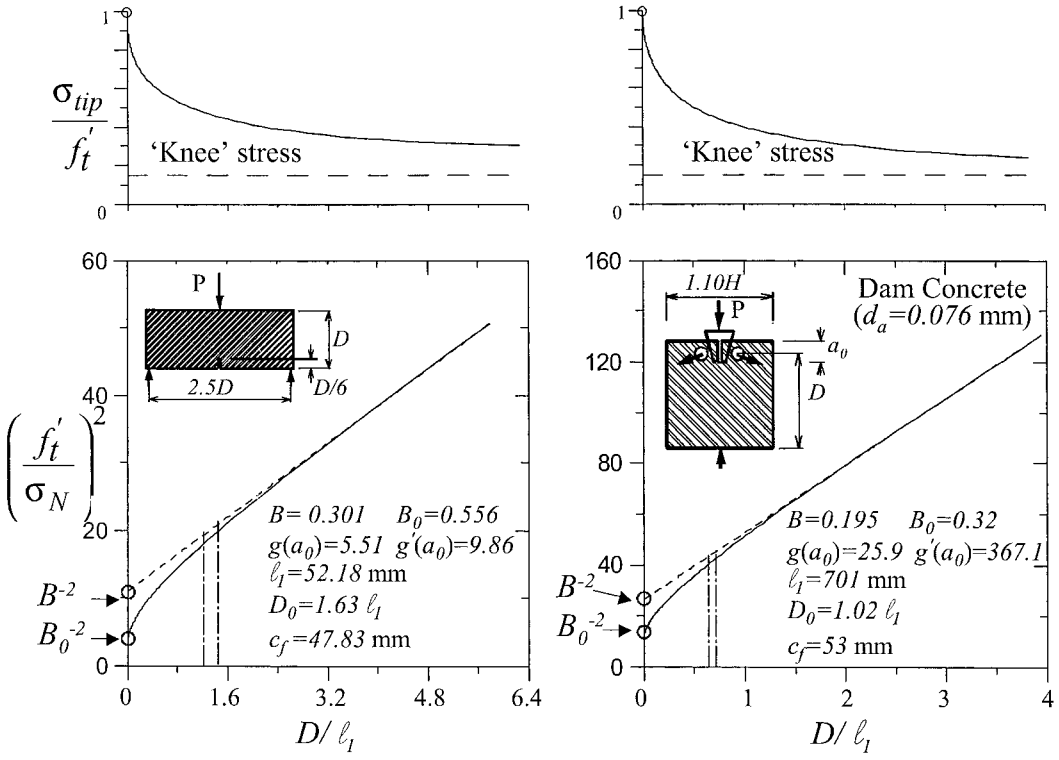

Figure 5. Continuation of Figure 4 for the three-point bend and wedge splitting specimens.

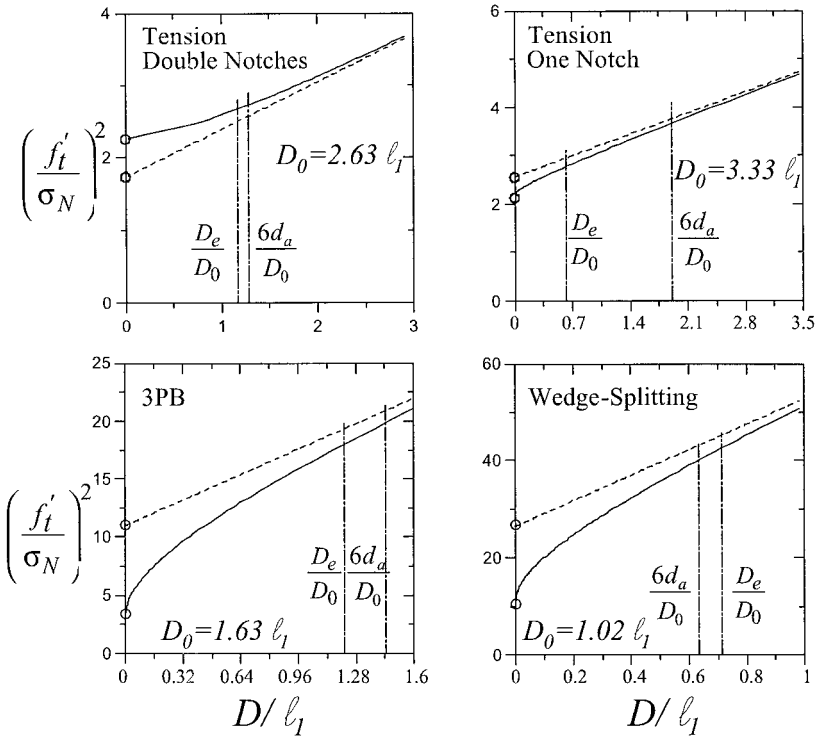

Figure 6. Plots from Figures 4 and 5 in expanded horizontal scale emphasizing the small-size behavior.

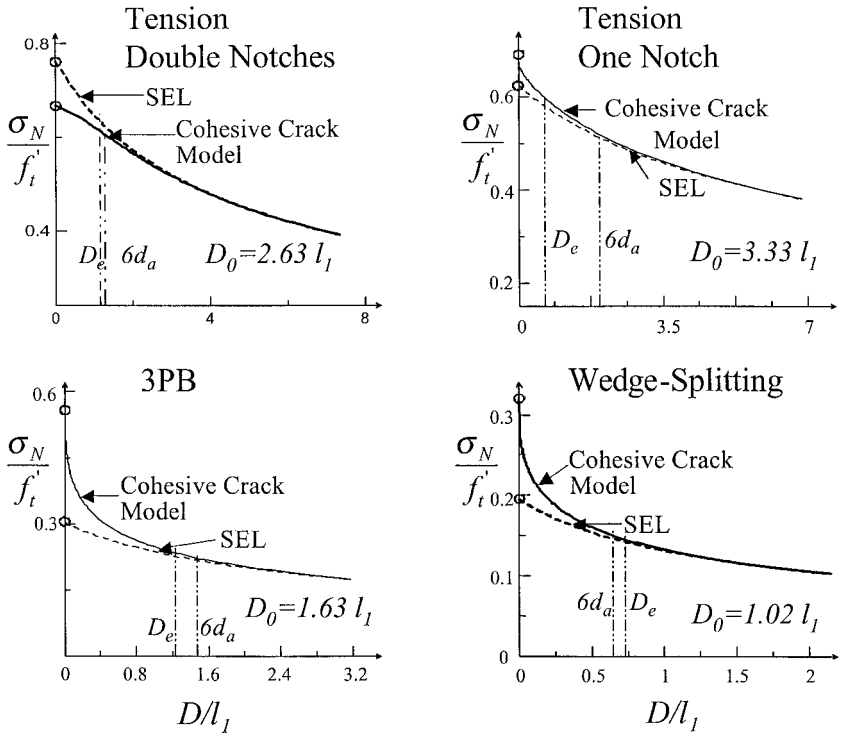

Figure 7. Size effect curves of the cohesive crack model and the classical size effect law (SEL, Bažant, 1984) plotted in different coordinates illuminating the small-size asymptotics.

plot (Figures 4 and 5). As one can see in the figures, $D_{\min}$ is larger than D_e for all the specimen geometries considered. So $D_{\min}$ lies within the range in which the classical size effect law is very close to the size effect of the cohesive crack model.

The last observation justifies the use of the classical size effect law for approximate evaluation of the fracture characteristics of the cohesive crack model from the maximum load values. According to Figure 6, the best specimen, for which the size effect of the cohesive crack model is the closest to the size effect law, is the singly or doubly edge-notched prism under axial tension. Such a specimen, unfortunately, is not the most convenient one for testing. For the most popular specimen, the three-point bend beam, the errors are not so small (nearly 3% of σ_N).

Despite the small errors of the size effect method, it is not more difficult, as shown by Guinea et al. (1994a,b), to evaluate the test data according to the exact solution of the cohesive crack model calculated in advance, once for all, for the chosen test geometry. Therefore, the use of this exact solution must be seen as preferable if the smallest specimens admissible for continuum mechanics should be used.

11. Improved direct and inverse formulae for the cohesive size effect curve

It will now be convenient to express the exact solution of the cohesive crack model in terms of the deviation $\Delta(\xi)$ from the size effect asymptote for $D \to \infty$;

$$\eta = \phi(\xi) = g\xi + p - \Delta(\xi), \tag{21}$$

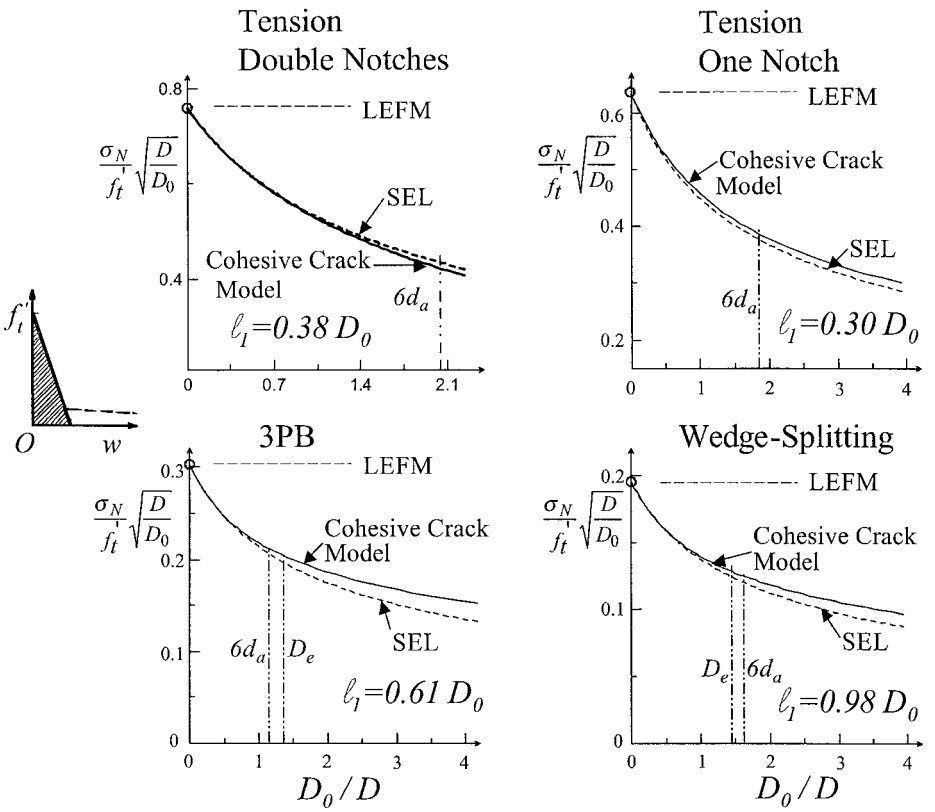

Figure 8. Size effect curves of the cohesive crack model and the classical size effect law (SEL, Bažant, 1984) plotted in different coordinates illuminating the large-size asymptotics.

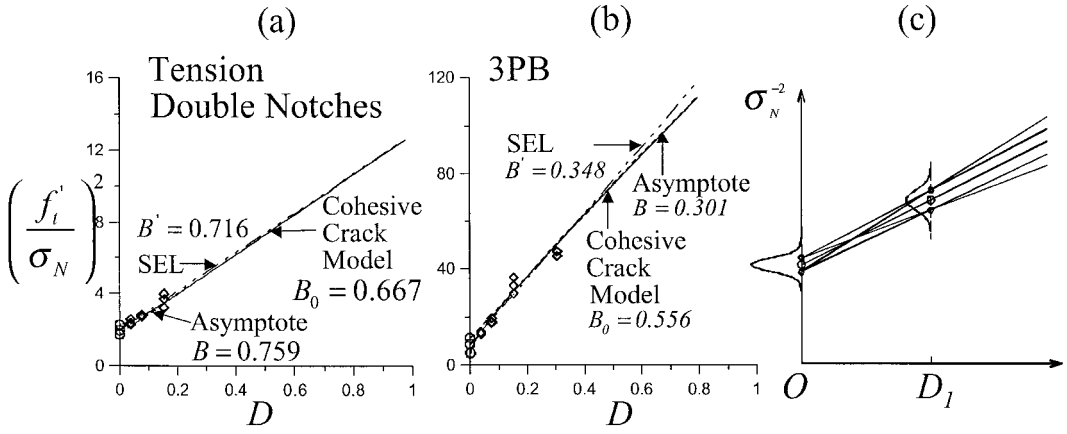

Figure 9. (a, b) Difference between size effect law fitted to test data and asymptotic size effect law of cohesive crack model, for direct tension specimens with two symmetric notches (a) and for three-point bend specimen (b). (c) Size effect lines connecting the points representing the mean ± standard deviation.

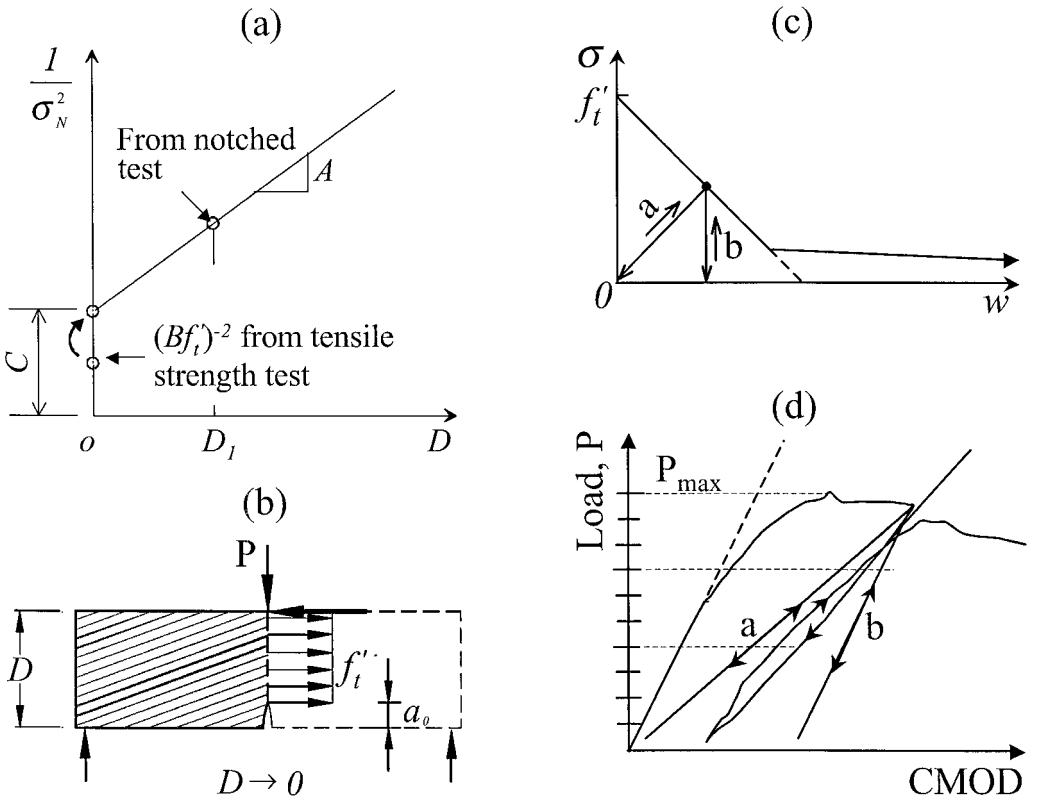

Figure 10. (a) Illustration of notched-unnnotched method. (b) Free-body diagram of one half of three-point bend specimen at $D; \to 0$. (c) Extreme cases of unloading-reloading lines used in simulations of Jenq–Shah method (TPFM) for softening stress-separation curve. (d) Extreme cases for load–CMOD diagram.

where $g = g(\alpha_0)$ = slope of the dimensionless size effect asymptote for the given geometry (dashed lines in Figures 4 and 5), and $p = B^{-2}$ = dimensionless intercept of this line with the vertical axis. The values of B^{-2}, $g = g(\alpha_0)$ and $g' = g'(\alpha_0)$) for the double and single notched tension specimens, the three-point bend (3PB) specimen and the wedge-splitting specimen considered here are listed in Figures 4 and 5.

Various simple polynomial or rational functions can be used to closely approximate $\Delta(\xi)$ over one order of magnitude of ξ. A very close approximation over the whole range $\xi \in (0, \infty)$ (Figure 11a and 11b) can be achieved with the following Dirichlet series:

$$\Delta(\xi) = \sum_{i=1}^{i=5} h_i \mathrm{e}^{-\xi/k_i}. \tag{22}$$

Here k_i are suitably chosen constants and h_i are parameters obtained by fitting. We now consider the 3PB geometry shown in Figure 11 (right) (which is chosen by ACI Committee 446 for a standard under preparation and slightly differs from the 3PB geometry used by Bažant and Pfeiffer, 1987, shown in Figure 5). Minimization of the sum of squared errors (taken at regular intervals in $\ln \xi$-scale) by Levenberg–Marquardt algorithm furnished the values $h_1 = 1.0905$, $h_2 = 2.530$, $h_3 = 6.879$, $h_4 = 16.26$, $h_5 = 0.05200$, $k_1 = 0.001443$, $k_2 = 0.01299$, $k_3 = 0.1169$, $k_4 = 1.052$, $k_5 = 9.469$. Note that, by definition of factors B

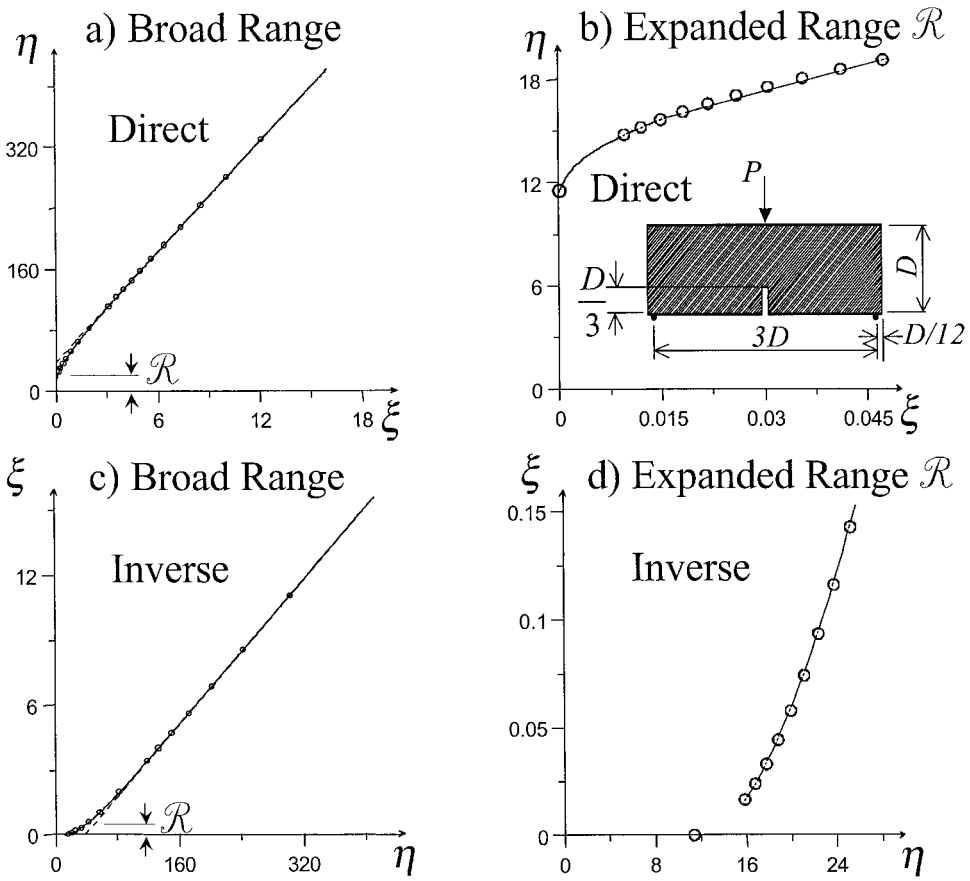

Figure 11. Comparison of the approximate formulae (21) (direct, on top) and (23) (inverse, at bottom) with the dimensionless size effect curves of cohesive crack model (solid curves) for 3PB beam (dashed lines: size effect asymptote).

and B_0, $h_1 + h_2 + h_3 + h_4 + h_5 = B^{-2} - {B_0}^{-2}$. Other accurate representations, possibly with fewer parameters, could doubtless be also devised.

For data evaluation, one further needs the inverse function, which may be best represented also by a deviation $\delta(\eta)$ from the size effect asymptote:

$$\xi = \psi(\eta) = \frac{\eta - p}{g} + \delta(\eta), \tag{23}$$

where

$$\delta(\eta) = \sum_{i=1}^{i=6} f_i \mathrm{e}^{-\eta/\kappa_i}. \tag{24}$$

Here κ_i are suitably chosen constants and f_i are parameters obtained by fitting; for the chosen 3PB specimen geometry $f_1 = 0.1905$, $f_2 = 0.3.236$, $f_3 = 0.2911$, $f_4 = 0.1253$, $f_5 = 0.07280$, $f_6 = 0.1102$, $\kappa_1 = 15.25$, $\kappa_2 = 19.07$, $\kappa_3 = 23.83$, $\kappa_4 = 29.79$, $\kappa_5 = 37.23$, $\kappa_6 = 46.55$.

Both formulae (21) and (23) are asymptotically exact for large sizes. Their relative errors $\Delta\xi/\xi$ must obviously decrease with increasing ξ or η since for $\eta \to 0$ the relative error $\Delta\eta/\eta$

must tend to ∞. For the ranges $\xi \in (0.015, \infty)$ and $\xi \in (2, \infty)$, the errors of the direct formula are within 0.8% and 0.06% of η, and for the ranges $\eta \in (16, \infty)$ and $\eta \in (100, \infty)$, the errors of the inverse formula (Figures 11c and 11d) are within 0.9% and 0.09% of ξ. Guinea et al.'s inverse formula is accurate within only about one order of magnitude of ξ (error 0.3% for $\eta \in (120, 580)$), although this is quite sufficient for the range of typical specimen sizes. For that range, the error of the present new inverse formula is about 4-times smaller, being within 0.08% of η. Admittedly, the present new formulae are broader and more accurate than necessary for test data evaluation, but their use is not more difficult than the use of Guinea et al.'s limited-range formulae. Besides, they may be useful for other kinds of calculations with the cohesive crack model.

The advantage of the present formulae is that they are only partly empirical. Their main part, the size effect asymptote, is theoretically based and is invertible exactly. Only the small deviation from the size effect asymptote is subjected to empirical approximation. The spirit of these formulae is not to discard the size effect method but to improve it.

Note that the cohesive crack model is closer to the size effect law when the bending moment transmitted by the ligament is small or zero (tensioned edge-notched specimens in Figure 5). When there is bending with a compressive stress at the ligament side opposite to the notch, there is a steeper drop in η and a higher negative curvature very close to the point $D = 0$ ($\xi = 0$).

12. Statistical analysis of notched and unnotched test data

Consider that we have ν randomly scattered tensile strength data, $f'_{t\,i}$ ($i = 1, 2, \ldots \nu$), and n randomly scattered data on the nominal strength of notched specimens of the same size D and the same geometry, $\sigma_{N\,j}$ ($j = 1, 2, \ldots n$). Aside from the trivial task of determining the statistics of tensile strength, the goal is to determine the mean value $\bar{G}_f$ of G_f and its coefficient of variation ω_{G_f}. Various methods of statistical evaluation can be conceived. The following method A′ represents a straightforward statistical generalization and size effect adaptation of the method proposed by Guinea et al. (1994a,b), which we labeled as method A.

12.1. Method A′ Monte Carlo simulation when only notched data are scattered

1. Calculate the mean tensile strength $\bar{f}'_t = \frac{1}{m}\sum_{i=1}^{m} f'_{t\,i}$ and then, for each of the notched tests ($j = 1, 2, \ldots n$), calculate $\eta_j = (\bar{f}'_t/\sigma_{N\,j})^2$ (see the η-value in Figure 12a).
2. For each notched test, calculate $\xi_j = \psi(\eta_j)$ (see the ξ-values in Figure 12a). Then calculate the fracture energy corresponding to each test $G_{f\,j} = D(\bar{f}'_t)^2 \,/\, \bar{E}'\xi_j$ ($j = 1, 2, \ldots n$), in which $\bar{E}'$ is the mean of E', and evaluate the mean $\bar{G}_f$ and the coefficient of variation $\omega^{\circ}_{G_f}$.
3. Now one needs estimate the effect of randomness of f'_t and E. Since these variables influence G_f in a multiplicative (rather than additive) form, we can very roughly estimate the overall coefficient of variation as

$$\omega_{G_f} = \sqrt{{\omega^{\circ}_{G_f}}^2 + \alpha_f {\omega_{f_t}}^2 + \alpha_E {\omega_E}^2} \tag{25}$$

(Benjamin and Cornell, 1970, Equation (2.4.130); Haldar and Mahadevan, 2000; Ang and Tang, 1975). Here ω_E is the coefficient of variation of Young's modulus of concrete, and α_f

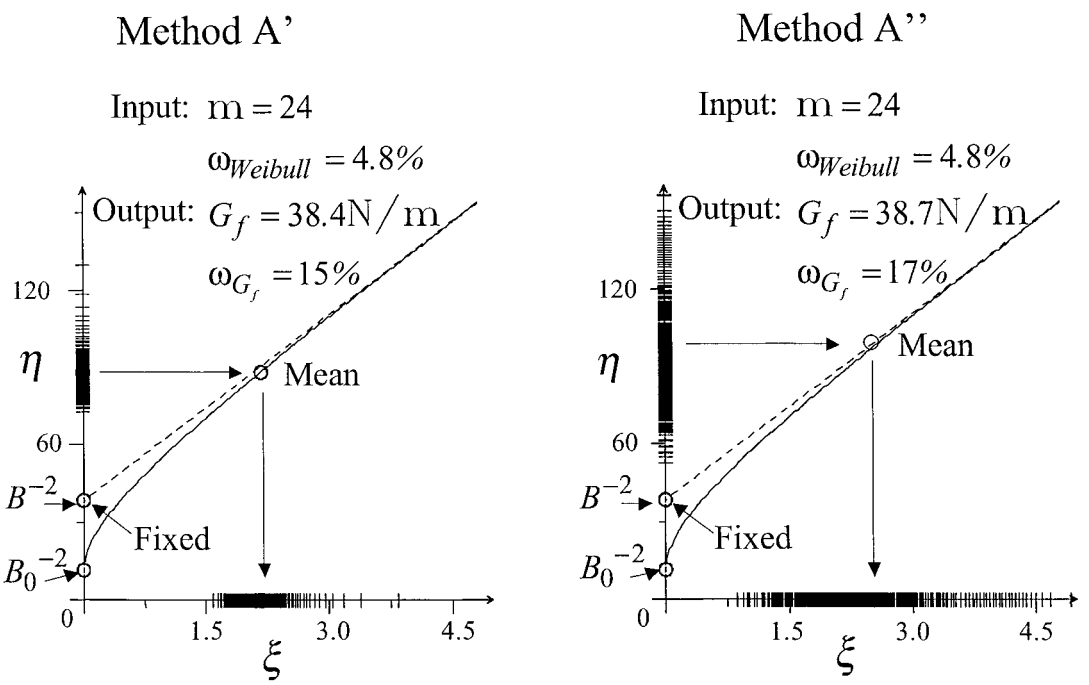

Figure 12. Left: illustration of statistical method A′ – from the random nominal strength data shown on the vertical axis one obtains a set of points of dimensionless sizes on the horizontal axis, each of which implies one value of ℓ_1 and of G_f. Right: illustration of Monte Carlo simulation (method A″) – from the nominal strength data calculated from the random pair of f_{ti} and σ_{Nj} one obtains a set of points of dimensionless sizes on the horizontal axis, each of which implies one value of ℓ_1 and of G_f.

and α_E are coefficients reflecting the degree of correlation; for $\alpha_f = \alpha_E = 0$, f_t' and E are perfectly correlated, and for $\alpha_f = \alpha_E = 1$ they are uncorrelated (or statistically independent). Little is known about the correlation properties of these characteristics of concrete, and the correlation coefficient is anyway highly uncertain. For the sake of numerical comparisons between various methods, we will assume that $\alpha_f = 1, \alpha_E = 0$ (although in reality the proper values of α_f and α_E lie surely between 0 and 1). Note, however, that in the statistical regression approach discussed later, which is made possible by exploiting the known systematic trend of size effect, the nagging question of statistical correlation of f_t' and G_f does not exist (which is a significant advantage of the regression approach).

12.2. Method A″ Monte Carlo simulation with randomness of both notched and strength data

1. For each nominal strength test j and each tensile strength test i, calculate $\eta_{ij} = (f'_{t\,i}/\sigma_{N\,j})^2$ $(i = 1, 2, \ldots \nu;\ j = 1, 2, \ldots n)$.
2. For each possible pair of i and j (each combination of all the data, defining all the points on the vertical axis in Figure 12b), calculate $\xi_{ij} = \psi(\eta_{ij})$ (see the ξ_{ij}-values in Figure 12b) and $G_{f\,ij} = D(f'_{t\,i})^2 \,/\, \bar{E}'\xi_{ij}$.
3. Calculate the mean $\bar{G}_f = \frac{1}{mn}\sum_i \sum_j G_{f\,ij}$ and the corresponding coefficient of variation $\omega^{\circ}_{G_f}$. Then estimate the overall coefficient of variation:

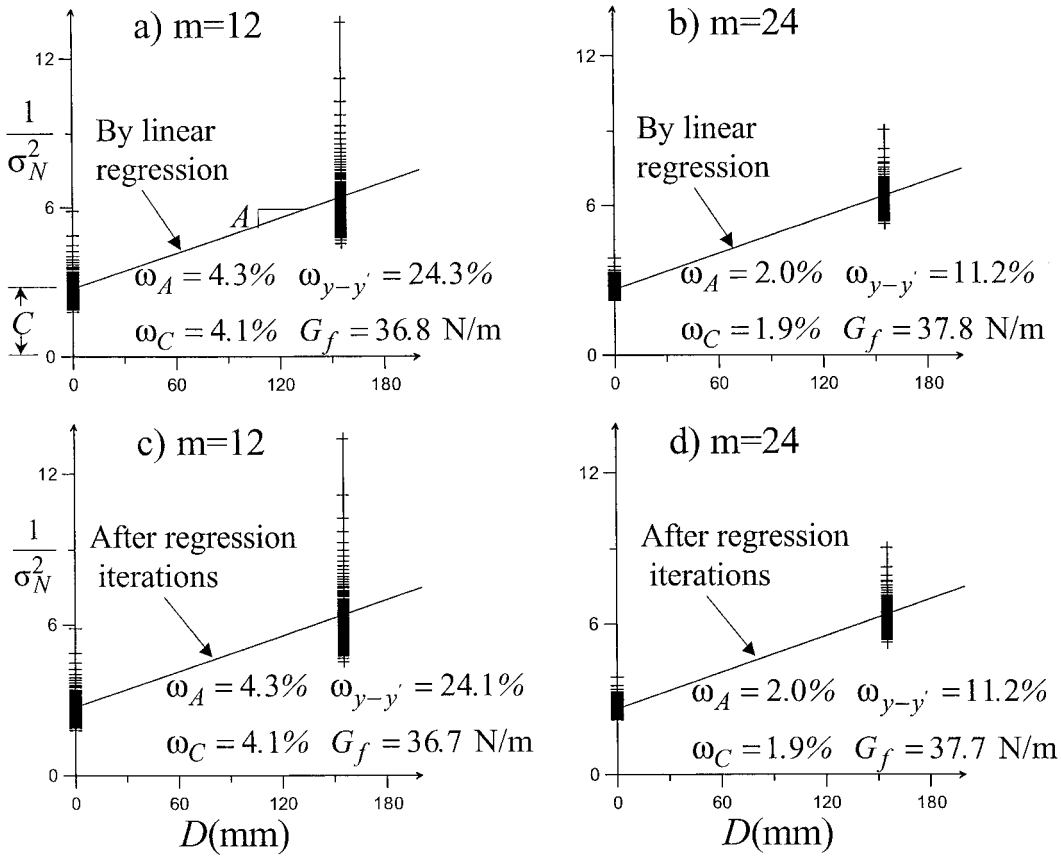

Figure 13. Identification of G_f and f_t' reduced to linear regression (100 randomly generated input data points for strength and 100 for nominal stress are shown on the vertical lines for $D = 0$ and $D = 155$ mm and yield the regression lines drawn and the coefficients of variation listed. Left: large scatter of input, right: small scatter. Top: simple regression. Bottom: iterated regression.

$$\omega_{G_f} = \sqrt{\omega_{G_f}^{\circ\,2} + \alpha_E \omega_E{}^2}. \tag{26}$$

Although α_f does not appear above, the uncertainty about the statistical correlation between σ_N and f_t' is not removed. Lacking information, we simply assume for all our numerical simulations that these variables are uncorrelated (statistically independent).

This method could further be extended by considering individually all the combinations with the measured values E_k' of E' ($k = 1, 2, \ldots \mu$), and then taking statistics of $n\nu\mu$ values $G_{f_{ijk}}$, although the troublesome question of correlation would again crop up.

12.3. Method B. Linear regression of data from notched and unnotched tests

If an underlying mean trend exists, the proper statistical approach is regression. As long as the cohesive crack model is valid, the trend is provided by the size effect. In the sense of size effect, we have at least two sizes: the actual size of notched specimens, and the theoretical size corresponding to the tensile strength test, which is, in the sense of the cohesive crack model, zero (Bažant and Li, 1996). Realizing this point leads us to the following algorithm.

1. Calculate the mean tensile strength $\bar{f}'_t = \frac{1}{m}\sum_{i=1}^{m} f'_{t\,i}$.
2. For each of the notched tests ($j = 1, 2, \ldots n$), calculate $\eta_j = (\bar{f}'_t/\sigma_{N\,j})^2$.
3. From (23) with (24), calculate $\xi_j = \psi(\eta_j)$ (location of the vertical line on the right of each plot on the top of Figure 13). Then calculate $\Delta_j = \Delta(\xi_j)$ ($j = 1, 2, \ldots n$).
4. Calculate the notched specimen data for linear regression:

$$Y_{\nu+j} = (\eta_j + \Delta_j)/(\bar{f}'_t)^2 \quad (j = 1, 2, \ldots n) \tag{27}$$

   (these are the points that would ideally lie on the size effect asymptote, Figure 13, if there were no scatter). Set $Y_i = 1/(B f'_{t\,i})^2$ ($i = 1, 2, \ldots \nu$).
5. Consider the standard linear regression relation $Y = AX + C$ of the size effect method (Figure 13, top) where $X = D$, and set $X_i = 0$ for $i = 1, 2, \ldots \nu$ and $X_i = D$ for $i = \nu + 1, \nu + 2, \ldots \nu + n$. Then run linear regression of all data points (X_i, Y_i), $i = 1, 2, \ldots \nu + n$, using the weights $w_i = 1/\nu$ for $i = 1, \ldots \nu$ and $w_i = 1/n$ for $i = \nu + 1, \nu + 2, \ldots N$ ($N = \nu + n$). The well known regression formulae yield the mean slope $\bar{A}$ and mean intercept $\bar{C}$, and also the coefficients of variation of regression slope and intercept, ω_A, ω_C where $\omega_A = [\sum_{i=1}^{N}(Y_i - Y'_i)^2/(N-2)]^{1/2}/\bar{Y}$, $\bar{Y} = \sum_{i=1}^{N}(Y_i - Y'_i)/N$ and $Y'_i = AX_i + C =$ values on the regression line.
6. Finally, according to formulae (14) and (15) of the size effect method, estimate the mean fracture energy and its coefficient of variation:[3]

$$\bar{G}_f \approx g(\alpha_0) / \bar{E}'\bar{A}, \qquad \omega_{G_f} \approx \sqrt{\omega_A^2 + \alpha_E \omega_E^2}. \tag{23}$$

Note that the use of statistical regression made possible by the underlying size effect trend bypasses the vexing uncertainty of the degree of statistical correlation between f'_t and G_f, expressed by coefficient α_f. But is it logical to assume the underlying size effect trend when one test corresponds to $D = 0$? Indeed it is, or else we would be denying continuity with respect to D. The size effect of cohesive crack model is continuous as the size D is decreased arbitrarily. Imposing some lower bound on D below which a discontinuity is imagined would certainly be irrational.

From the regression illustration in Figure 9c, it is clear that if point D_1 is moved to the right, the scatter of the slopes diminishes. This means that the larger the notched specimen size D, the smaller is the uncertainty of the regression line slope A. Consequently, the error of G_f decreases when the notched specimen size is increased.

For this reason, the specimens should be as large as practical (of course, they should not be so large that σ_{tip} would no longer be higher than the 'knee' point on the bilinear softening curve, Figures 4 and 5; but this could hardly ever happen in practice).

12.4. Method B′. Linear regression improved by iteration

A minor weak point of the foregoing regression method B is that the initial calculation of ξ_j is based on the mean tensile strength of unnotched tests, disregarding the scatter of ℓ_1 and ξ due to tensile strength randomness. In this regard, method B may be remedied as follows.

[3]More accurately, $\bar{G}_f = g(\alpha_0) M_E M_A$ where M_E and M_A are the means of $1/E'$ and $1/A$ (Benjamin and Cornell, 1970, Section 2.4); $M_A = \bar{A}^{-1}(1 + 2\omega_A^2) \neq \bar{A}^{-1}$ because $A^{-1} = \bar{A}^{-1} - \bar{A}^{-2}(A - \bar{A}) + 2\bar{A}^{-3}(A - \bar{A})^2 - \ldots$.

1. Using the classical size effect method (method B* described later), get the first estimates $\bar{G}_f$, $\bar{c}_f$ and $\bar{f}'_t = \sqrt{\bar{E}'\bar{G}_f/[g'(\alpha_0)\bar{c}_f]}\,/B$.
2. Skipping step 1, run the other linear regression steps according to Method B, and then obtain new values of $\bar{G}_f$, $\bar{c}_f$ and $\bar{f}_t$.
3. Repeat the foregoing step until a specified convergence criterion is reached (see the converged regression line shown at the bottom of Figure 13). Then obtain ω_{G_f} as in the last step of Method B.

12.5. Method B″. Generalization of regression to multiple notched sizes

As in the classical size effect method, the accuracy and reliability of measurements including unnotched strength tests may be improved by using different sizes of notched specimens. Sometimes data for specimens of S different sizes D_s ($s = 1, 2, \ldots S$) for the same concrete may be available from different laboratories. While methods A, A′ and A″ are inapplicable to such situations, method B using regression may be easily generalized.

1. Calculate the mean tensile strength $\bar{f}'_t = \frac{1}{m}\sum_{i=1}^{m} f'_{t\,i}$.
2. For notched tests $j = 1, 2, \ldots n_S$ of each size $s = 1, 2, \ldots S$, calculate $\eta_j^s = (\bar{f}'_t/\sigma^s_{N\,j})^2$ where superscript s labels sizes s.
3. From (23) with (24), calculate for all data for each size $\xi_j^s = \psi(\eta_j^s)$, and then calculate $\Delta_j^s = \Delta(\xi_j^s)$ ($j = 1, 2, \ldots n_S, s = 1, 2, \ldots S$).
4. Calculate the notched specimen data for linear regression:

$$Y_{\nu+j,s} = (\eta_j^s + \Delta_j^s)/(\bar{f}'_t)^2 \qquad (j = 1, 2, \ldots n_S, s = 1, 2, \ldots S) \tag{29}$$

5. Set $Y_{i,0} = 1/(B f'_{t\,i})^2$ ($i = 1, 2, \ldots \nu$).
6. Consider the standard linear regression relation $Y = AX + C$ of the size effect method (Figure 14 left), where $X = D_s$, and set $X_{i,0} = 0$ for $i = 1, 2, \ldots \nu$ and $X_{i,s} = D_s$ for $i = \nu + 1, \nu + 2, \ldots \nu + n_S, s = 1, 2, \ldots S$. Then run linear regression of all data points $(X_{i,s}, Y_{i,s})$, $i = 1, 2, \ldots \nu + n_s, s = 1, 2, \ldots n_S$, using the weights $w_{i,0} = 1/\nu$ for $i = 1, \ldots \nu$ and $w_{i,s} = 1/n_S$ for $i = \nu + 1, \nu + 2, \ldots \nu + n, s = 1, 2, \ldots n_S$. The regression yields the mean slope $\bar{A}$ and mean intercept $\bar{C}$, and the coefficients of variation of slope and intercept, ω_A, ω_C.
7. Finally, estimate the mean fracture energy and its coefficient of variation from (28).

12.6. Method B‴. Generalization of regression to multiple notched shapes and sizes

Another way to improve the accuracy of results is to use dissimilar notched specimens, either with one specimen size or with multiple sizes. Although not as helpful for accuracy as varying the specimen size, it is nevertheless useful to cut notches of different depths (different α) in specimens of one size (which avoids the burden of casting beams of different depths). To make linear regression possible (Bažant, 2002a) (11) can be rewritten as $g_i D_i + g'_i c_f - E' G_f \sigma_{Ni}^{-2} = 0$ where subscripts $i = 1, 2, \ldots s$ label the specimens, and the right-hand side is zero only for theoretically perfect data. Division by $E' G_f g'_i$ provides the linear regression equation equation: $Y = AX + C$ where

$$Y = \frac{1}{g'_i \sigma^2_{Ni}}, \qquad X = \frac{g_i D_i}{g'_i}, \qquad A = \frac{1}{E' G_f}, \qquad C = \frac{c_f}{E' G_f}. \tag{30}$$

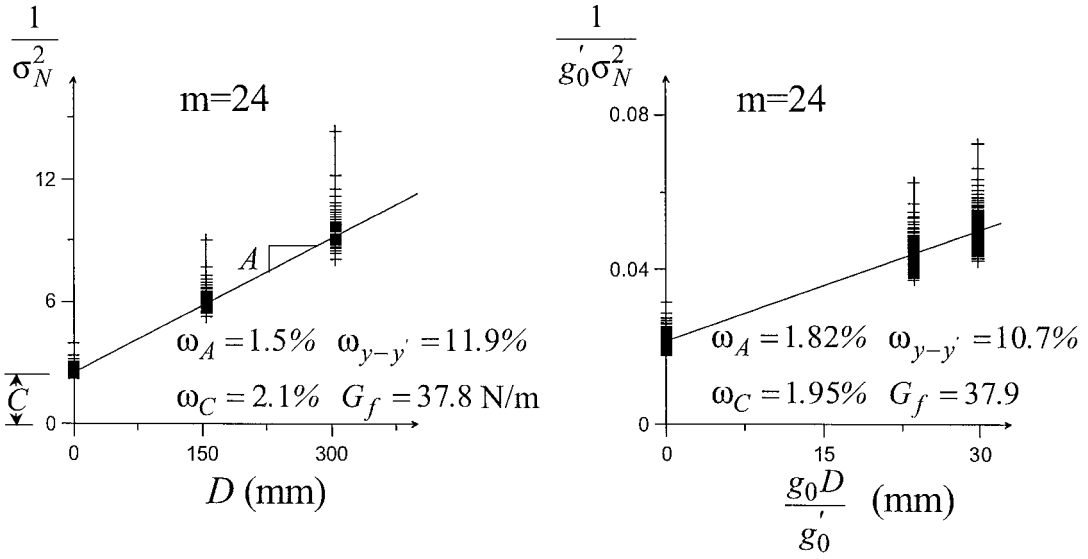

Figure 14. Left: illustration of statistical method B extended to multiple notched sizes. Right: illustration of statistical method B extended to multiple notched shapes.

One needs to obtain the direct and inverse formulae for each relative notch length. The following algorithm may be used:

1. First carry out steps 1 and 2 of method B″. Then use (23) and (24) with different parameter values for the chosen different shapes to calculate $\xi_j^s = \psi_s(\eta_j^s)$ for each shape, and then calculate $\Delta_j^s = \Delta_s(\xi_j^s)$ $(j = 1, 2, \ldots n_S, s = 1, 2, \ldots S)$.
2. Calculate the notched specimen data for linear regression:

$$Y_{v+j,s} = (\eta_j^s + \Delta_j^s)/[(g_s)'_j(\bar{f}_t')^2] \quad (j = 1, 2, \ldots n_S, s = 1, 2, \ldots S) \tag{31}$$

3. Set $Y_{i,0} = 1/[(g_s)'_j(Bf'_{ti})^2]$ $(i = 1, 2, \ldots v)$.
4. Run linear regression with $X_j, s = g_j^s D^s/(g^s)'_j$ for $j = 1, 2, \ldots n_S$ and $s = 1, 2, \ldots S$, obtain the mean slope $\bar{A}$ and mean intercept $\bar{C}$, and the coefficients of variation of slope and intercept, ω_A, ω_C (Figure 14 right).
5. Finally, using (30), estimate the mean fracture energy and its coefficient of variation:

$$\bar{G}_f \approx 1 \,/\, E'\bar{A}, \qquad \omega_{G_f} \approx \sqrt{\omega_A^2 + \alpha_E \omega_E^2} \tag{32}$$

[again, a more accurate result may be obtained in a way similar to the footnote at (23)].

12.7. Method C. Nonlinear regression of f_t' and σ_N data

The fracture parameters can also be obtained by simultaneous nonlinear optimization of the fits of all notched and unnotched test data combined. The values of G_f and f_t' are two unknowns to be optimized by minimizing the sum of squares of errors of the formulae compared to the test data. Very effective for that purpose is the Levenberg–Marquardt nonlinear optimization algorithm available as a standard computer library subroutine. However, the algorithm converges to the correct result only if a good enough initial estimate is supplied

as the input. The algorithm also furnishes estimates of the coefficients of variation, but in the case of nonlinear regression they are normally not statistically unbiased estimates and are accurate only if the errors are sufficiently small.

1. The first step is to use the classical size effect method, same as step 1 of method B′, to obtain the initial estimates of $\bar{G}_f$ and $\bar{f}'_t$ to be supplied as input to the Levenberg–Marquardt subroutine.
2. Supply to Levenberg-Marquardt subroutine the functions

$$\begin{aligned} Y_i &= BX_1 - f'_{t\,i} \quad (i = 1, 2, \ldots \nu), \\ Y_{\nu+j} &= \phi\left(\frac{DX_1{}^2}{\bar{E}'X_2}\right) X_1 - \sigma_{N\,j} \quad (j = \nu+1, \nu+2, \ldots \nu+n), \end{aligned} \tag{33}$$

   where $X_1 = f'_t$ and $X_2 = G_f$ are two optimization unknowns.
3. Minimizing the sum $\sum_{i=1}^{\nu+n} Y_i{}^2$, the algorithm furnishes as output the optimum values of $X_1 = f'_t$ and $X_2 = G_f$ and the estimates of ω_{f_t} and ω_{G_f}.
4. Finally, make the correction $\omega_{G_f} \leftarrow \sqrt{\omega_{G_f}{}^2 + \omega_{E}{}^2}$.

As an alternative to the last step, if individual scattered test data on E' are available one could include the errors in E' as additional functions Y_i and consider $X_3 = E'$ as a third optimization unknown.

Like regression, this method, too, can be easily extended to multiple sizes or geometries of notched specimens.

13. Numerical comparison of statistical methods

We need large statistical samples of the f'_t and σ_N data with purely random variation. For the sake of comparison, it is better to generate such samples numerically than experimentally. Theoretically, the statistical distributions of both f'_t and σ_N must have Weibull tails (e.g., Bažant, 2001b), and so we assume Weibull distributions throughout the whole range. The Weibull modulus m is functionally related to the coefficient of variation; $\omega^2 = \Gamma(1 + 2m^{-1})\Gamma^{-2}(1 + m^{-1}) - 1$. Choosing equal sample sizes, $\nu = n$, for both $f'_{t\,i}$ and $\sigma_{N\,j}$, we subdivide each Weibull cumulative distribution into n horizontal strata of equal thickness, i.e., of equal probability content. Then we use a random number generator to obtain random stratum numbers. To each generated stratum number we assign the value of f'_t or σ_N as the value for the mid-height of the stratum, in order to obtain random samples $f'_{t\,i}$ and $\sigma_{N\,j}$ (i, $j = 1, 2, N$). We choose the sample size $n = 100$ for f'_t and σ_N each, and we assume the averages $\bar{f}'_t = 3.8$ MPa and $\bar{\sigma}_N = 0.41$ MPa. We generate the samples randomly according to the Weibull distributions which are fully characterized by their means and coefficients of variation ω_f and ω_{σ_N}. We consider two cases, one with $\omega_f = \omega_{\sigma_N} = 10.3\%$, which corresponds Weibull modulus $m = 12$, and another with $\omega_f = \omega_{\sigma_N} = 4.8\%$, which corresponds to Weibull modulus $m = 24$. We analyze a three-point bend specimen of depth $D = 155$ mm (shown in Figure 11). Further we choose $\bar{E}' = 27.5$ GPa (which gives the characteristic length $\ell_1 = 72$ mm) and $\omega_E = 0$ (i.e., we ignore the scatter of E', and thus need not decide the value of α_f). For method A′ we also need the value of α_f, and we simply choose $\alpha_f = 1$ (i.e., assume no statistical correlation). For the Monte Carlo simulation in method A″, we generate 10^4 pairs by considering all the combinations of each $f'_{t\,i}$ value with each $\sigma_{N\,j}$ value, and thus we obtain as output 10^4 values of $G_{f\,ij}$.

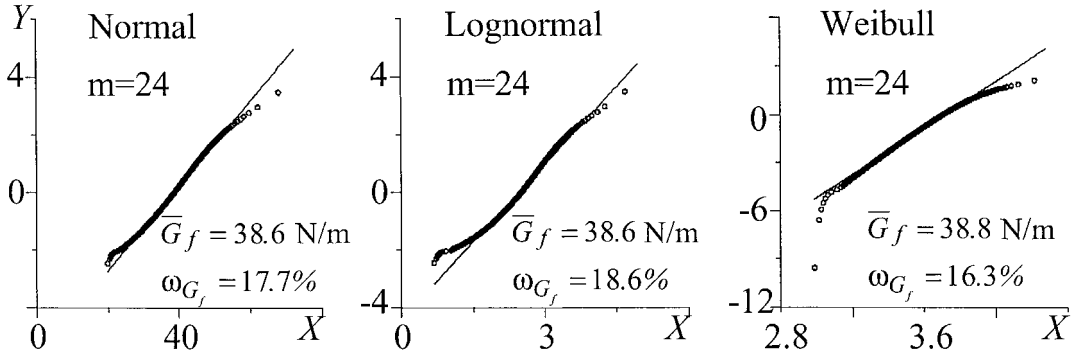

Figure 15. Fitting of cumulative probability curve of G_f assuming (a) normal, (b) lognormal, and (c) Weibull distributions.

The results of the computations are summarized in Tables 1 and 2. It is seen that all the methods yield similar mean predictions, although the results of method A′, equivalent to the original Guinea et al.'s method A, are slightly out of line. For the coefficients of variation, large differences are found. ω_{G_f} is the coefficient of the individual values based on each (f_t', σ_N) pair, which however makes no sense for the regression methods B and B′; $\omega_{\bar{G}f}$ is the coefficient of variation of the mean $\bar{G}_f$, which is not listed for method A″ because the number of pairs (f_t', σ_N) (which is 10^4) is much larger than the sample size for the other methods (it is known that, approximately, $\omega_{\bar{G}f} \propto N^{-1/2}$), where N = number of pairs, and $\lim_{N\to\infty} \omega_{\bar{G}f} = 0$. The coefficients of variation ω_{G_f} of individual G_f values are not listed for methods B and B′ because the individual values do not figure in the regression approach.

The results of the computations by all the methods are summarized in Tables 1 and 2. We see that the means $\bar{f}_t'$ and $\bar{G}_f$ calculated by methods B, B′ and C are almost same. The last line of the table for each m value shows for comparison the results obtained with the size effect method based on the zero size and the notched specimen size (which is equivalent to regression method B if one sets $\Delta(\xi) = \delta(\eta) = 0$).

In method A″, Monte Carlo simulation, the output is a very large sample of $G_{f_{ij}}$ values, numbering $N = 10^4$. Ordering these values from the smallest to the largest, one can construct the cumulative probability curve of G_f. According to the order k in the sample, one can estimate the cumulative probability, $F(G_{f_k})$ $(k = 1, 2, \ldots, 10^4)$. We use the popular Bernard's approximation to the median rank, $F(G_{f_k}) = (k - 0.3)/(N + 0.4)$.

It is interesting to check how closely $F(G_{f_k})$ can be approximated by the normal, lognormal and Weibull distributions. To this end, we may calculate the graph of each cumulative distribution on the so-called 'probability paper' which transforms the distribution into a straight line. The closeness of the graphs of $F(G_{f_k})$ in Figure 15 to a straight line indicates how well each distribution can describe the randomness of G_f. Numerically this may be characterized by a linear regression of the data points in Figure 15, which provides the values of correlation coefficient r and coefficient of variation $\omega^*_{G_f}$ about the regression line listed in Table 1(c). All the three distributions provide good approximations but the $\omega^*_{G_f}$ value for the Weibull distribution is the smallest one, while both $\omega^*_{G_f}$ and G_f are similar to the values obtained by Monte Carlo method. Thus the Weibull distribution seems to describe the G_f distribution best.

Table 1. Statistical evaluation and comparison of results

Input data	$f_t' = 3.8$ MPa, $G_f = 38$ N/m, $E' = 27.5$ GPa							
A. Results for $m = 12$ ($\omega = 10.3\%$)								
Method	$\bar{f}_t'$ (MPa)	$\bar{G}_f$ (N/m)	ω_A	ω_C	ω_{f_t}	ω_{G_f}	$\omega_{y-y'}$	$\omega_{\bar{G}_f}$
A	–	38.2	–	–	–	–	–	–
A′	–	39.7	–	–	–	29.0%	–	2.9%
A″	–	41.1	–	–	–	36.5%	–	–
B	–	36.8	4.3%	4.1%	–	–	24.3%	4.3%
B′	3.74	36.7	4.3%	4.1%	–	–	24.1%	4.3%
C	3.74	36.9	–	–	32.0%	38.0%	33.0%	–
B*(SEM)	–	38.4	4.7%	4.3%	–	–	25.9%	4.7%
TPFM(a)	–	39.5	–	–	–	–	–	–
TPFM(b)	–	30.1	–	–	–	–	–	–
B. Results for input $m = 24$ ($\omega = 4.80\%$)								
Method	$\bar{f}_t'$ (MPa)	$\bar{G}_f$ (N/m)	ω_A	ω_C	ω_{f_t}	ω_{G_f}	$\omega_{y-y'}$	$\omega_{\bar{G}_f}$
A	–	38.2	–	–	–	–	–	–
A′	–	38.4	–	–	–	15.0%	–	1.5%
A″	–	38.7	–	–	–	17.0%	–	–
B	–	37.8	2.0%	1.9%	–	–	11.2%	2.0%
B′	3.78	37.7	2.0%	1.9%	–	–	11.2%	2.0%
C	3.78	37.8	–	–	15.0%	18.0%	15.5%	–
B*(SEM)	–	39.3	2.2%	2.0%	–	–	11.9%	2.2%
TPFM(a)	–	39.5	–	–	–	–	–	–
TPFM(b)	–	30.1	–	–	–	–	–	–

C. Approximation of the results for G_f with three distributions

Distribution type	$m = 24$			$m = 12$		
	r^2	$\bar{G}_f$ (MPa)	$\omega^*_{G_f}$	r^2	$\bar{G}_f$ (MPa)	$\omega^*_{G_f}$
Normal	0.994	38.6	17.7%	0.932	40.8	39.2%
Lognormal	0.968	38.6	18.6%	0.964	41.1	38.6%
Weibull	0.982	38.8	16.3%	0.963	41.0	38.4%

For the sake of comparison, Tables 1A and 1B also give the results obtained with the size effect method (SEM) based on only two sizes, size D and the zero size (which corresponds to setting $\Delta(\xi) = \delta(\eta) = 0$). The differences from method B or B′, the best method, are seen to be quite small for the mean, and almost nil for the coefficients of variation. Obviously, if the normal engineering accuracy is sufficient, SEM can be used.

In practice, the number of tests would normally be much less than 100. Consider now small data samples, with 3 or 6 tests in each sample of notched or unnotched specimens. The question is how reliable the statistics from such samples are. For this reason we now compare

Table 2. Statistical comparison for small samples ($m = 24$, $\omega_{\text{Weibull}} = 4.8\%$)

	6 sample set					3 sample set				
	A′	A″	B	B′	C	A′	A″	B	B′	C
$\overline{f_t}$ (MPa)	–	–	3.80	3.79	3.79	–	–	3.80	3.79	3.79
$\overline{G_f}$ (N/m)	38.5	38.7	38.0	38.0	38.0	38.5	38.7	38.1	38.1	38.2
$\omega_{\bar{f}_t}$	–	–	2.3%	2.4%	2.4%	–	–	3.1%	3.1%	3.1%
$\omega_{\bar{G}_f}$	7.6%	7.6%	8.3%	8.3%	8.3%	8.6%	8.7%	9.7%	9.6%	9.6%
$\max(\bar{f}'_{t_i})$	–	–	3.94	3.94	3.94	–	–	4.05	4.05	4.05
$\min(\bar{f}'_{t_i})$	–	–	3.48	3.49	3.49	–	–	3.48	3.48	3.48
$\max(\bar{G}_{f_i})$	45.8	46.8	46.7	46.3	46.4	48.0	48.0	48.7	48.1	48.2
$\min(\bar{G}_{f_i})$	30.1	31.2	29.9	29.7	29.8	29.6	29.9	27.7	27.6	27.8

the results for very many samples of 3 or 6 each. We generate 600 random data values for the tensile strength and 600 for the notched nominal strength. From these we generate randomly 100 sets of 6 or 3 data each. The results of computations are summarized in Table 2, in which $\overline{f_t}$ or $\overline{G_f}$ denote the overall mean of all the individual means $\bar{f}'_{t,i}$ or $\bar{G}_{f,i}$ for the individual sets $i = 1, 2, \ldots, 100$. From the tables we note that, in each method, the coefficient of variation of the sample mean is significantly smaller for the samples of size 6 than for the samples of size 3, and is only a little large than that for the sample of size 100, as seen in Table 1. The overall means $\overline{f_t}$ and $\overline{G_f}$ of all the sample means of 6 or 3 (first 2 lines in Table 2) are identical, as of course expected. The same observation follows from the last four lines of Table 2 which compare, between samples of sizes 6 and 3, the maxima and minima of the means of the individual samples. So we confirm the well known fact that the samples of size 6 provide at least a crude (albeit exaggerated) information on the general scatter, while the samples of size 3 are useless for characterizing the scatter.

14. Approximate size effect regression using tensile strength and notched specimens of one size

The magnitude of the correction of the cohesive crack model to the size effect law (SEL) is illustrated in Figures 9a and 9b for two typical test specimens in the normal size range, and also documented by comparison with the rows B*(SEM) in Tables 1A and 1B. The correction is seen to be relatively small. This means that if only the rough engineering accuracy is desired, the corrections $\Delta(\xi)$ and $\delta(\eta)$ may be skipped, i.e., one may set $\Delta(\xi) = \delta(\eta) = 0$. In other words, the size effect method (SEM) can be used in step 3 of method B, in step 2 of method A″ (instead of $\psi(\xi)$), and in steps 3 and 4 of method B″, basing calculation simply on the classical size effect law (11), labeled 'SEM' in Figures 9a and 9b. The regression method, method B, thus reduces to the following method B* proposed in Bažant and Li (1996) and named 'zero-brittleness' size effect method (because the unnotched specimens for strength testing have a zero brittleness number).

14.1. METHOD B*. ZERO-BRITTLENESS VERSION OF SIZE EFFECT METHOD (SEM)

1. Calculate the mean tensile strength $\bar{f}'_t = \frac{1}{m}\sum_{i=1}^{m} f'_{t\,i}$.
2. For each of the notched tests ($j = 1, 2, \ldots, n$), calculate $\eta_j = (\bar{f}'_t/\sigma_{N\,j})^2$. Then calculate the notched specimen data for linear regression: $Y_{\nu+j} = \eta_j/(\bar{f}'_t)^2$ ($j = 1, 2, \ldots n$). Set $Y_i = 1/(B f'_{t\,i})^2$ ($i = 1, 2, \ldots \nu$).
3. Consider the standard linear regression relation $Y = AX + C$ of the size effect method (Figure 13, top) where $X = D$, and set $X_i = 0$ for $i = 1, 2, \ldots \nu$ and $X_i = D$ for $i = \nu + 1, \nu + 2, \ldots \nu + n$. Then run linear regression of all data points (X_i, Y_i), $i = 1, 2, \ldots \nu + n$, using the weights $w_i = 1/\nu$ for $i = 1, \ldots \nu$ and $w_i = 1/n$ for $i = \nu + 1, \nu + 2, \ldots N (N = \nu + n)$. The well known regression formulae yield the mean slope $\bar{A}$ and mean intercept $\bar{C}$, and also the coefficients of variation of regression slope and intercept, ω_A, ω_C.
4. Finally, according to formulae (14) and (15) of the size effect method, estimate the mean fracture energy $\bar{G}_f$ and its coefficient of variation ω_{G_f}; $\bar{G}_f \approx g(\alpha_0)/\bar{E}'\bar{A}$, $\omega_{G_f} \approx \sqrt{\omega_A^2 + \alpha_E \omega_E^2}$.

If one needs only the means, without statistics, then one may skip the regression and calculate the means $\bar{\sigma}_N$ and $\bar{\sigma}_0$ of all the experimental values of σ_N and σ_0, and then simply estimate the mean G_f and c_f according to the size effect law as

$$G_f = \frac{g(\alpha_0) D_1}{E'(\bar{\sigma}_N^{-2} - \bar{\sigma}_0^{-2})}, \qquad c_f = \frac{g(\alpha_0) D_1}{g'(\alpha_0)[(\bar{\sigma}_0/\bar{\sigma}_N)^2 - 1]}. \tag{34}$$

15. Ambiguity of TPFM Due to Unloading

In the TPFM, one needs to measure the unloading-reloading response of cracked specimen near the maximum load in order to estimate the effective crack length. This aspect is not theoretically consistent with the cohesive crack model. The fracture energy, defined as the area under the softening curve, is as a matter of principle independent of the unloading and reloading properties of the cohesive crack. The fracture energy G_f (as well as G_F) if fully characterized by softening curve for loading only, and has nothing to do with the unloading curve (Figure 10c). Therefore, the unloading stiffness of cracked specimens should not be considered in determining the fracture energy.

To document the problems caused by the use of unloading, the cohesive crack model characterized by the input data of the preceding computations (first line in Table 1) was further used for a numerical simulation of the fracture test according to Jenq–Shah method (TPFM). This required computation of the diagram of the load versus the crack mouth opening displacement (δ_{CMOD}) of the 3PB specimen shown in Figure 10c (except for the cohesive crack, all the material of specimen was considered as linearly elastic). In addition, it was necessary, according to the definition of TPFM, to simulate unloading and reloading from a post-peak state in which the load is reduced to 95% of the previous peak load. Using these computational results, the G_f was calculated exactly as specified in TPFM method. Since the unloading stiffness of cracked concrete is uncertain and quite variable, two different assumptions about the unloading-reloading stiffness were made, as shown by lines a and b in Figure 10c, and the corresponding results are listed in the rows TPFM(a) and TPFM(b) of Table 1. Both results are rather different from the input value $G_f = 38.0$ N/m.

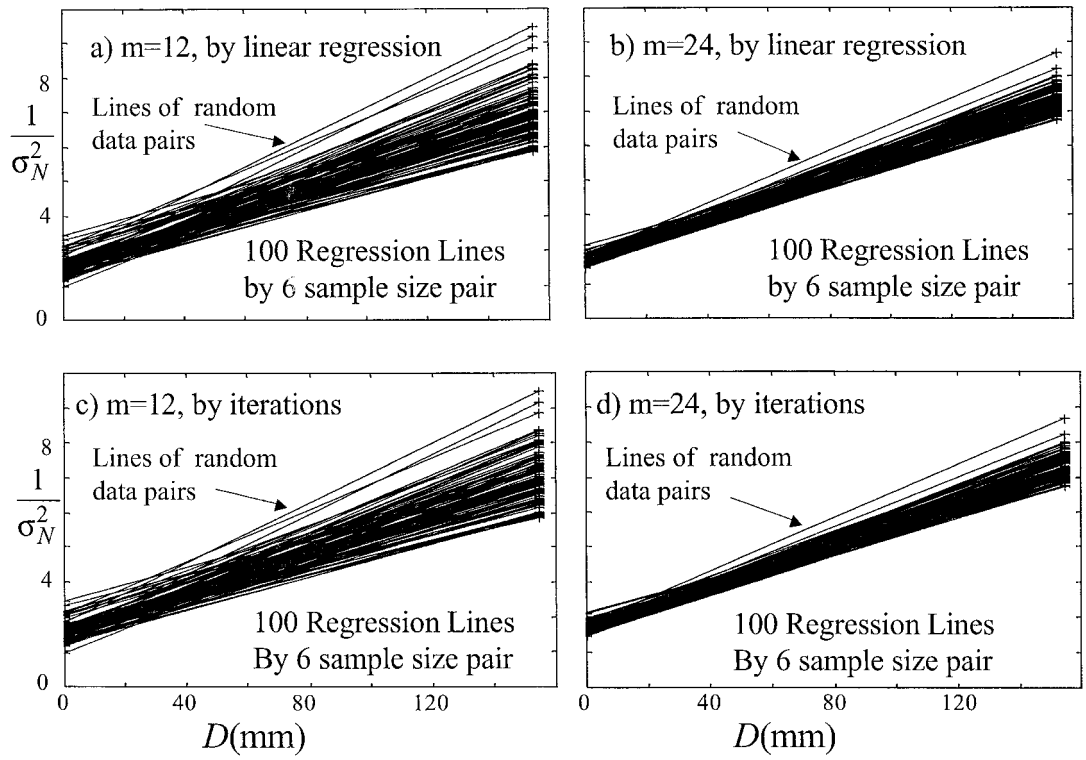

Figure 16. 100 size effect lines obtained (after cohesive model correction) for all the pairs of small size random input of unnotched strength values and small size random input of notched nominal strength values (Left: high scatter; Right: low scatter. Top: sets of 3 data each. Bottom: sets of 6 data each).

The result $G_f = 39.5$ N/m, obtained for crack unloading and reloading along to the line through the origin (line a Figure 10c), is 31% higher than the result $G_f = 30.1$ N/m, obtained for a vertical crack unloading and reloading (line b in Figure 10c) (in the load-deflection diagram, Figure 10d, the former corresponds again to unloading toward the origin, and the latter to unloading with the initial elastic stiffness of the notched specimen). Ideally, if no tiny fragments accumulated between the faces of the microcracks in the cohesive (fracture process) zone, and if all the microscopic slips in this zone were perfectly reversible, one would get line a in Figure 10c. If the microcrack closing were completely blocked by fragments between the microcrack faces, and if all the microscopic slips were totally irreversible, one would get line b.

Now it must of course be admitted that the lines a and b in Figuresd 10c and 10d are theoretical extremes. The real unloading-reloading stiffness is somewhere between, but it can nevertheless vary from one concrete to another through perhaps a half of the range between the extreme cases a and b, causing variations up to 15% depending on the amount and type of the aforementioned fragments and on the degree of irreversibility of frictional slips. This can be a source of significant ambiguity in the results of TPFM. The TPFM would be a completely sound method only if it could be proven that the unloading-reloading stiffness is uniquely determined by E, f_t' and G_f, but this is of course not true.[4]

[4]The TPFM has further significant disadvantages: (1) It is less simple to perform because, unlike the measurement of G_f by Guinea et al.'s method, it necessitates a stiff loading system, a servo-controlled testing machine, and

Note the difference between a quasibrittle material such as concrete and a brittle-ductile metal. The Wells-Cottrell method, which inspired TPFM, is free of the problems of TPFM because the nonlinear zone surrounding at the crack front in metals is almost entirely a plastic yielding zone while the fracture process zone forms only a negligible part of the nonlinear zone. Consequently, the unloading-reloading stiffness is always the initial elastic stiffness of the cracked metallic specimen, which is constant.

16. Conclusions

1. The level I fracture test of concrete should yield the initial fracture energy G_f (the area under the initial tangent of cohesive softening curve) rather than the total fracture energy G_F (the area under the whole curve), for two reasons: (a) The measurements of G_F exhibit a much larger statistical scatter than the measurements G_f; and (b) the maximum loads of normal structures are governed by G_f rather than G_F while the inference of G_f from G_F is highly uncertain and introduces a large additional statistical error into the maximum load prediction.
2. The method of Guinea et al. (1994a,b), which uses maximum load tests of notched specimens of only one size (and one geometry) and also Brazilian split-cylinder tests of tensile strength, is a simple, robust and user-friendly approach to establish G_f. However, the statistical correlation between G_f and the tensile strength f_t' is difficult to assess and creates a problem for statistical evaluation. The difficult problem of statistical correlation can be bypassed by statistical regression based on a known trend.
3. If the cohesive crack model is accepted as valid, the tensile strength data correspond to the zero size limit of the nominal strength of notched specimens because, for this limit, the nominal strength of a notched specimen can be calculated from f_t' alone. This means that, together with the tensile strength data, one has experimental data on the nominal strength for two specimen sizes – the actual size of notched specimens and the zero size. Hence, there exists a size effect trend, which can be exploited for statistical regression. The main advantage of te regression approach is that it circumvents the difficulty with statistical correlation between the notched test data and the unnotched strength test data (or between stochastic variables F_f and f_t'), and also makes possible refinements based on the knowledge of size effect law.
4. Thanks to the fact that the cohesive stress at notch tip is never reduced into the tail portion of the softening bilinear stress-separation curve of the cohesive crack model for concrete, the size effect method can be easily improved by introducing corrections based on exact solutions for the cohesive crack model. In the improved version, the size effect method is based on two sizes: (a) the size of notched specimen and (b) a zero size which corresponds to the tensile strength tests.
5. If the random scatter of experiments is ignored, the improved size effect method is exactly equivalent to Guinea et al.'s method. In that case one considers only one value of tensile

precise deformation control. (2) Consequently it is more prone to errors, which makes it less suitable for simple quality control tests in the field. (3) It provides no additional information that would not be provided by the Guinea et al.'s method. (4) The initial behavior of the crack band model (as well as the nonlocal and gradient models), which has generally become the basis of the computation of load capacities of structures, is calibrated by Guinea et al. method directly, but by TPFM only indirectly, through approximate LEFM relations of K_{Ic}^s and δ_{CTOD} to G_f and f_t' that involve an unnecessary (albeit small) error.

strength and one value of the nominal strength on notched specimens of one size and one shape, both taken as their mean values.

6. Although its improvements of mean predictions are small, the improved size effect method (method B of B′) has significant advantages for statistical evaluation of scattered test data compared to a straightforward statistical generalization of Guinea et al.'s method (method A′):
   - The notched and unnotched test data can be evaluated jointly by linear regression, which is the most robust statistical approach.
   - The regression setting, made possible by the known size effect trend, bypasses the question of statistical correlation between f_t' and G_f, which is always problematic. This is an important advantage of the regression approach.
   - The coefficient of variation of mean G_f obtained from regression is more realistic and substantially different than that obtained from the generalized Guinea et al.'s method—method A' (e.g., compare 4.30% to 2.90% in Table 1A, an error of 48%).
   - The coefficient of variation of deviations from the regression line, $\omega_{y-y'}$, is a more realistic measure of scatter of individual G_f values than the coefficient of variation ω_{G_f} based solely on the scatter of the notched tests because G_f depends not merely on the notched test data but equally on both the notched and unnotched test data. The differences between these two measures of scatter are large (the value 15.0% in Table 1B is 34% larger than 11.2%, and 29.0% in Table 1A is 19% larger than 24.3%).
7. The statistical regression exploiting the size effect trend has further the advantage that the accuracy and reliability of results may be easily enhanced by testing specimens with different notch lengths (and the same size), or specimens of different sizes.
8. The zero-brittleness version of the size effect method (method B*, Bažant and Li 1996), which also necessitates only one size of notched specimens, is equivalent to a simplification of Guinea et al.'s method. The mean G_f value obtained is less accurate, but adequate for most engineering purposes. The coefficient of variation is more realistic because the regression is used.
9. It is estimated that the ambiguity of Jenq-Shah method (TPFM) due to variations of unloading-reloading properties from one cracked concrete to another can cause errors with a spread up to about 15% of G_f (as estimated from K_c).

Acknowledgments

This study was funded under Grant 0740-350-A447 from the Infrastructure Technology Institute of Northwestern University funded by U.S. Department of Transportation. The background research was partly funded under Grant CMS-0732791 from the U.S. National Science Foundation to Northwestern University.

Appendix I. 'Plastic' crack for calculating σ_N for $D \to 0$

In the limit of $D \to 0$, the cohesive crack model is equivalent to a specimen consisting of two elastic parts joined at the crack plane by an infinitely thin layer of a 'glue' that is rigid–perfectly plastic in tension and has an infinite strength in compression. This was shown numerically by Planas and co-workers (see Bažant and Planas, 1998) and may be rigorously

proven by the asymptotic expansion of the cohesive crack formulation for a general boundary value problem (Bažant, 2001, 2002b).

Note that the 'glue' should not be assigned a finite compression strength. The reason is that one deals with a zero-size extrapolation from real specimens whose cross section measures at least several aggregate sizes. The compression stresses on the crack plane never reach the strength limit, and so the crack line 'glue' represents a connection infinitely strong in compression. A smooth extrapolation to zero size must preserve this property. Besides, the cohesive crack model does not include any compressive strength limit for the bulk material. Consequently, when compression stresses are needed on the crack plane to balance the load (which happens when the notched cross section is subjected to a sufficiently large bending moment), then these stresses must localize on the crack line into a concentrated compressive force.

As an example, consider the three-point bend specimen shown in Figure 10 (right). In the zero size limit, $\sigma = f_t' =$ uniform distribution through the entire ligament except that a concentrated compression force $F_c = b(D - a_0) f_t'$ acts at the compression face ($a_0 =$ notch depth, $D =$ beam depth). The bending moment in the notched cross section is $M = \frac{1}{2} b(D - a_0)^2 f_t'$, the applied load is $P_{\max} = 4M/L$, and the nominal strength in the zero-size limit is

$$\lim_{D \to 0} \sigma_N = \sigma_{N0} = 2 f_t'(D - a_0)^2 / LD. \tag{35}$$

This value (used before by Planas) represents the left end point of the size effect curve of the cohesive crack model in Figure 5 (left). For D less than about six aggregate sizes, this curve is of course not real but theoretical.

References

Ang, A. H.-S. and Tang, Wilson H. (1975). *Probability Concepts in Engineering Planning and Design*. J. Wiley, New York (Eq. 4.44a).

Barenblatt, G.I. (1959). The formation of equilibrium cracks during brittle fracture. General ideas and hypothesis, axially symmetric cracks. *Prikl. Mat. Mekh.* **23** (3), 434–444.

Barenblatt, G.I. (1962). The mathematical theory of equilibrium cracks in brittle fracture. *Advanced Appl. Mech.* **7**, 55–129.

Bažant, Z.P. (1984). Size effect in blunt fracture: Concrete, rock, metal. *J. of Engrg. Mechanics*, ASCE **110**, 518–535.

Bažant, Z.P. (1987). Fracture energy of heterogeneous material and similitude. Preprints, *SEM-RILEM Int. Conf. on Fracture of Concrete and Rock* (held in Houston, Texas, June 1987), (edited by Shah S.P. and Swartz, S.E.) SEM (Soc. for Exper. Mech.), pp. 390–402.

Bažant, Z.P. (2001). Size effects in quasibrittle fracture: Apercu of recent results. *Fracture Mechanics of Concrete Structures* (Proc., FraMCoS-4 Int. Conf., Paris), (edited by de Borst, R., Mazars, J., Pijaudier-Cabot, G. and van Mier, J.G.M.) Swets & Zeitlinger (A.A. Balkema Publishers), Lisse, pp. 651–658.

Bažant, Z.P. (2001b). Probabilistic modeling of quasibrittle fracture and size effect. *Proc., 8th Int. Conf. on Structural Safety and Reliability (ICOSSAR), held at Newport Beach, Cal., 2001)*, (edited by Corotis, R.B.), Swets & Zeitinger (Balkema), pp. 1–23.

Bažant, Z.P. (2002a). Concrete Fracture Models: Testing and Practice. *Engineering Fracture Mechanics* **69** (2), 165–206 (special issue on Fracture of Concrete and Rock, M. Elices, ed.).

Bažant, Z.P. (2002b). *Scaling of structural strength.* Hermes–Penton, London.

Bažant, Z.P. and Becq-Giraudon, E. (2001). Estimation of fracture energy from basic characteristics of concrete. *Fracture Mechanics of Concrete Structures* (Proc., FraMCoS-4 Int. Conf., Paris), (edited by de Borst, R., Mazars, J., Pijaudier-Cabot, G. and van Mier, J.G.M.), Swets and Zeitlinger (A.A. Balkema Publishers), Lisse, pp. 491–495.

Bažant, Z.P. and Becq-Giraudon, E. (2001). Statistical prediction of fracture parameters of concrete and implications for choice of testing standard. *Cement and Concrete Research* **32** (4), 529–556.

Bažant, Z.P. and Gettu, R. (1992). Rate effects and load relaxation: Static fracture of concrete. *ACI Materials Journal* **89** (5), 456–468.

Bažant, Z.P. and Kazemi, M.T. (1990). Determination of fracture energy, process zone length and brittleness number from size effect, with application to rock and concrete. *Int. J. of Fracture* **44**, 111–131.

Bažant, Z.P. and Li, Z. (1996). Zero-brittleness size-effect method for one-size fracture test of concrete. *J. of Engrg. Mechanics ASCE* **122** (5), 458–468.

Bažant, Z.P. and Oh, B.-H. (1983), Crack band theory for fracture of concrete. *Materials and Structures (RILEM, Paris)* **16**, 155–177.

Bažant, Z.P. and Pfeiffer, P.A. (1987). Determination of fracture energy from size effect and brittleness number. *ACI Materials Journal* **84**, 463–480.

Bažant, Z.P. and Planas, J. (1998). *Fracture and Size Effect in Concrete and Other Quasibrittle Materials*. CRC Press, Boca Raton and London (Sections. 9.2, 9.3)

Benjamin, J.R. and Cornell, C.A. (1970). *Probability, Statistics and Decision for Civil Engineers*. McGraw-Hill Book Co., New York.

Cottrell, A.H. (1963). *Iron and Steel Institute Special Report* 69, p. 281.

Elices, M., Guinea, G. V. and Planas, J. (1992) Measurement of the fracture energy using three-point bend tests: Part 3—Influence of cutting the $P - \delta$ tail. *Materials and Structures,* **25**, 327–334.

Elices, M., Planas, J. and Guinea, G.V. (1993). Modeling cracking in rocks and cementitious materials. *Fracture and Damage of Concrete and Rock*, (edited by Rossmanith, H.P.), E & FN Spon, London, pp. 3–33.

Elices, M. and Planas, J. (1996). Fracture mechanics parameters of concrete, an overview. *Advanced Cement-Based Materials* **4**, 116–127.

Gettu, R., Bažant, Z.P. and Karr, M.E. (1990). Fracture properties and brittleness of high-strength concrete. *ACI Materials Journal* **87** (Nov.-Dec.), 608–618.

Guinea, G.V., Planas, J. and Elices, M. (1992) Measurement of the fracture energy using three-point bend tests: Part 1—Influence of experimental procedures. *Materials and Structures* **25**, 212–218.

Guinea, G.V., Planas, J. and Elices, M. (1994a). Correlation between the softening and the size effect curves. *Size Effect in Concrete Structures*. (edited by Mihashi, H., Okamura, H. and Bažant, Z.P.), E&FN Spon, London, pp. 233–244.

Guinea, G.V., Planas, J. and Elices, M. (1994b). A general bilinear fitting for the softening curve of concrete. *Materials and Structures* **27**, 99–105 (also summaries in Proc., IUTAM Symp., Brisbane 1993 and Torino, 1994).

Guinea, G.V., Elices, M. and Planas, J. (1997). On the initial shape of the softening function of cohesive materials. *Int. J. of Fracture* **87**, 139–149.

Haldar, A. and Mahadevan (2000). *Probability, Reliability and Statistical Methods in Engineering Design.* J. Wiley, New York.

Hillerborg, A., Modéer, M. and Petersson, P.E. (1976). Analysis of crack formation and crack growth in concrete by means of fracture mechanics and finite elements. *Cem. and Concr. Res.* **6**, 773–782.

Guinea, G.V., Planas, J. and Elices, M. (1994). Correlation between the softening curve and the size effect curves. *Size Effect in Concrete Structures*, (edited by Mihashi, H., Okamura, H. and Bažant, Z.P.), E & FN Spon, London, pp. 233–244.

He, S., Plesha, M.E., Rowlands, R.E. and Bažant, Z.P. (1992). Fracture energy tests of dam concrete with rate and size effects. *Dam Engineering* **3** (2), 139–159.

Hillerborg, A., Modéer, M. and Petersson, P.E. (1976). Analysis of crack formation and crack growth in concrete by means of fracture mechanics and finite elements. *Cem. Concr. Res.* **6**, 773–782.

Hillerborg, A. (1983). Examples of practical results achieved by means of the fictitious crack model, in *Preprints, Prager Symp. on Mechanics of Geomaterials: Rocks, Concretes, Soils*, (edited by Bažant, Z.P.), Northwestern University, Evanston, pp. 611–614.

Hillerborg, A. (1985a). The theoretical basis of method to determine the fracture energy G_f of concrete. *Materials and Structures* **18** (106), 291–296.

Hillerborg, A. (1985b). Results of three comparative test series for determining the fracture energy G_f of concrete. *Materials and Structures* **18** (107).

Jenq, Y.S. and Shah, S.P. (1985). A two parameter fracture model for concrete. *Journal of Engineering Mechanics* **111**(4), 1227–1241.

Kfouri, A.P. and Rice, J.R. (1977). Elastic-plastic separation energy rate for crack advance in finite growth steps. *Fracture 1977* (Proc., 4th Int. Conf. on Fracture, ICF4, Waterloo), (edited by Taplin, D.M.R.), Univ. of Waterloo, Ontario, Canada, Vol. 1, pp. 43–59.

Knauss, W.C. (1973). On the steady propagation of a crack in a viscoelastic sheet; experiment and analysis. *The Deformation in Fracture of High Polymers*, (edited by Kausch, H.H.), Plenum, New York, pp. 501–541.

Knauss, W.C. (1974). On the steady propagation of a crack in a viscoelastic plastic solid. *J. of Appl. Mech. ASME* **41** (1), 234–248.

Leonov, M.Y. and Panasyuk, V.V. (1959). Development of a nanocrack in a solid (in Russian). *Prikladnaya Mekhanika* (Soviet Applied Mechanics) **5** (No. 4), 391–401; English translation in *A tropical encyclopedia of current knowledge* (edited by G.P. Cherepanov), Krieger Publ., Malabur, FL (1998).

Nallathambi, P. and Karihaloo, B.L. (1986), Determination of specimen-size independent fracture toughness of plain concrete. *Mag. of Concrete Res.* **38** (135), 67–76.

Nakayama, J. (1965). Direct measurement of fracture energies of brittle heterogeneous material. *J. of the Amer. Ceram. Soc.* **48** (11).

Palmer, A.C. and Rice, J.R. (1973), The growth of slip surfaces on the progressive failure of over-consolidated clay. *Proc. Roy. Soc. Lond. A*. **332**, 527–548

Petersson, P.E. (1981). Crack growth and development of fracture zones in plain concrete and similar materials. *Report* TVBM-1006, Div. of Building Materials, Lund Inst. of Tech., Lund, Sweden.

Planas, J., Guinea, G.V. and Elices, M. (1993). Softening curves for concrete and structural response. *Fracture and Damage of Concrete and Rock*, (edited by Rossmanith, H.P.), E & FN Spon, London, pp. 66–75.

Planas, J., Guinea, G.V. and Elices, M. (1997). Generalized size effect equation for quasibrittle materials. *Fatigue and Fracture of Engineering Materials and Structures* **20** (5), 671–687.

Planas, J., Guinea, G.V. and Elices, M. (1999). Size effect and inverse analysis in concrete fracture. *Intern. J. of Fracture* **95**, 367–378.

Planas, J., Elices, M. and Guinea, G.V. (1992) Measurement of the fracture energy using three-point bend tests: Part 2—Influence of bulk energy dissipation. *Materials and Structures* **25**, 305–312.

Rice, J.R. (1968). Mathematical analysis in the mechanics of fracture. *Fracture—An advanced treatise*, Vol. 2, (edited by Liebowitz, H.), Academic Press, New York, pp. 191–308.

RILEM (1985) Recommendation TC 50-FMC. Determination of fracture energy of mortar and concrete by means of three-point bend tests of notched beams. *Materials and Structures* **18** (106), 285–290.

RILEM (1990a) Recommendation TC 89-FMT. Size effect method for determining fracture energy and process zone of concrete. *Materials and Structures* **23**, 461–465.

RILEM (1990b) Recommendation TC 89-FMT. Determination of fracture parameters (K_I^s and CTOD_c) of plain concrete using three-point bend tests. *Materials and Structures* **23**, 461–465.

Rocco, C.G. (1996). Influencia del Tamaño y Mecanismos de Rotura del Ensayo de Compresión Diametral. Doctoral Thesis, Universidad Politecnica de Madrid, Spain.

Smith, E. (1974). The structure in the vicinity of a crack tip: A general theory based on the cohesive crack model. *Engineering Fracture Mechanics* **6**, 213–222.

Tang, T., Bažant, Z.P., Yang, S. and Zollinger, D. (1996). Variable-notch one-size test method for fracture energy and process zone length. *Engineering Fracture Mechanics* **55** (3), 383–404.

Tattersall, H.G. and Tappin, G. (1966). The work of fracture and its measurement in metals, ceramics and other materials. *J. of Mater. Sci.* **1** (3), 296–301.

Wells, A.A. (1961). Unstable crack propagation in metals-cleavage and fast fracture. *Symp. on Crack Propagation*, Cranfield, Vol.1, 210–230.

Wittmann, F.H., Rokugo, K., Brühwiller, E., Mihashi, H. and Simopnin, P. (1988). Fracture energy and strain softening of concrete as determined by compact tension specimens. *Materials and Structures (RILEM, Paris)* **21**, 21–32.

Wnuk, M.P. (1974). Quasi-static extension of a tensile crack contained in viscoelastic plastic solid. *J. Appl. Mech. ASME* **41** (1), 234–248.